Journal of Catalysis **197,** 251–266 (2001)
doi:10.1006/jcat.2000.3092, available online at http://www.idealibrary.com on IDEAL®

Hole-Doped $La_{1.85}Sr_{0.15}CuO_{4-\delta}X_\sigma$ (X = F, Cl) and Electron-Doped $Nd_{1.85}Ce_{0.15}CuO_{4-\delta}X_\sigma$ Halo-Oxide Catalysts for the Selective Oxidation of Ethane to Ethene

H. X. Dai, C. F. Ng, and C. T. Au[1]

Department of Chemistry and Center for Surface Analysis and Research, Hong Kong Baptist University, Kowloon Tong, Hong Kong

Received April 7, 2000; revised August 11, 2000; accepted October 17, 2000; published online December 21, 2000

The catalytic performance and characterization of $Ln_{1.85}A_{0.15}CuO_{4-\delta}$ and $Ln_{1.85}A_{0.15}CuO_{4-\delta}X_\sigma$ (Ln = La, Nd; A = Sr, Ce; X = F, Cl) for the oxidative dehydrogenation of ethane (ODE) to ethene have been investigated. The hole-doped catalysts performed better than the electron-doped ones. Under the reaction conditions of temperature, 660°C; $C_2H_6/O_2/N_2$ molar ratio, 2/1/3.7; and contact time, 1.67×10^{-4} h g mL^{-1}; $La_{1.85}Sr_{0.15}CuO_{3.930}Cl_{0.053}$ showed 82.8% C_2H_6 conversion, 73.2% C_2H_4 selectivity, and 60.6% C_2H_4 yield; $Nd_{1.85}Ce_{0.15}CuO_{3.981}F_{0.092}$ showed 72.1% C_2H_6 conversion, 61.8.0% C_2H_4 selectivity, and 44.6% C_2H_4 yield. The sustainable performance during a period of 60 h on-stream reaction at 660°C demonstrated that the F- and Cl-doped catalysts are durable. The results of X-ray powder diffraction indicated that the Sr-substituted cuprates were of T structure whereas the Ce-doped cuprates were of T' structure. The results of X-ray photoelectron spectroscopic (XPS) studies revealed that there were Cu^{2+} and Cu^{3+} in the Sr-doped cuprate catalysts and Cu^{+} and Cu^{2+} in the Ce-doped cuprate catalysts. The results of the XPS, thermogravimetric analysis (TGA), and $^{18}O_2$-pulsing studies demonstrated that the incorporation of halide ions into the $Ln_{1.85}A_{0.15}CuO_{4-\delta}$ lattice promoted the activity of lattice oxygen. By comparing the results of XPS, TGA, and O_2 temperature-programmed desorption with the catalytic performance of the catalysts, we conclude that (i) lattice O^{2-} species at the surface are active for the selective oxidation of ethane; (ii) in excessive amount, O^- species accommodated in oxygen vacancies are prone to induce the total oxidation of ethane; and (iii) a suitable Cu^{3+} or Cu^{+} concentration and/or oxygen nonstoichiometry in $Ln_{1.85}A_{0.15}CuO_{4-\delta}X_\sigma$ are required for the best catalytic performance of the catalysts.

Key Words: **ethane selective oxidation; ethene generation; oxidative dehydrogenation; ODE reaction; superconducting materials $La_{1.85}Sr_{0.15}CuO_{4-\delta}$ and $Nd_{1.85}Ce_{0.15}CuO_{4-\delta}$; perovskite-related oxide catalyst; halo-oxide $La_{1.85}Sr_{0.15}CuO_{4-\delta}X_\sigma$ and $Nd_{1.85}Ce_{0.15}CuO_{4-\delta}X_\sigma$.**

INTRODUCTION

Ethane is the second largest component of natural gas and is one of the main products in the oxidative coupling of methane (OCM). It is of significance to convert ethane to ethene since ethene is the starting material for the synthesis of many value-added chemicals. In the past decades, the oxidative dehydrogenation of ethane (ODE) to ethene has been investigated intensively and extensively. Many compounds have been tested as catalysts for this reaction. Among them, Dy_2O_3/Li^+–MgO–Cl^- (ca. 57% C_2H_4 yield at 570°C) (1), Mo–V–Nb–Sb–Ca–O (ca. 52% C_2H_4 yield at 400°C) (2), and LiCl/sulfated zirconia (ca. 68% C_2H_4 yield at 650°C) (3) seem to be highly effective. Although $KSr_2Bi_3O_4Cl_6$ gave a C_2H_4 yield of ca. 70% at 640°C, the catalyst deteriorated due to Cl leaching (4). In recent years, many researchers have reported the use of perovskite-type oxides such as $SrCo_{0.8}Li_{0.2}O_3$ (5), $SrCo_{0.8}Fe_{0.2}O_3$ and $La_{0.8}Sr_{0.2}CoO_3$ (6), $La_{0.6}Sr_{0.4}Co_{0.8}Fe_{0.2}O_3$ (7), and $La_{2-x}Sr_xCuO_{4-\delta}$ and $Nd_{2-x}Ce_xCuO_{4-\delta}$ (8) as catalysts for OCM reactions, and $La_{1-x}Sr_xFeO_{3-\delta}$ (9) for ODE reactions. They all displayed moderate catalytic performance. Yi *et al.* claimed that under the reaction conditions of temperature, 650°C; C_2H_6/O_2 molar ratio, 1/1; and contact time = 1.43×10^{-4} h g mL^{-1}; $SrFeO_{3-\delta}$ showed 87% C_2H_6 conversion, 43% C_2H_4 selectivity, and 37% C_2H_4 yield (9).

Perovskite-type oxides (ABO_3) exhibit good activity for the total oxidation of carbon monoxide and hydrocarbons (10, 11). The oxygen vacancies and redox property of these materials play crucial roles in catalyzing the complete oxidation reactions. Generally speaking, a perovskite-type oxide catalyst with higher oxygen vacancy density and stronger redox ability performs better. By incorporating halide ions with ionic radii similar to O^{2-} ions to the oxygen vacancies, one could decrease the oxygen vacancy density and strengthen the redox ability and hence convert these combustion materials to catalysts selective for the oxidation of ethane to ethene. Putting this idea into practice, we have generated several classes of halide-doped perovskite-type and perovskite-related (K_2NiF_4-type) oxide catalysts. In our previous studies, we have characterized and reported $La_{1-x}Sr_xFeO_{3-\delta}X_\sigma$ (X = F, Cl) (12), $SrFeO_{3-\delta}Cl_\sigma$ (13), and $YBa_2Cu_3O_{7-\delta}X_\sigma$ (14) catalysts, which showed good activity and durability for the ODE reaction. Since the discovery

[1] To whom correspondence should be addressed. Fax: 852-2339-7348. E-mail: pctau@hkbu.edu.hk.

0021-9517/01 $35.00

of hole-doped (with holes being the charge carriers) high-temperature superconductor (HTSC) $La_2CuO_{4-\delta}$ (15) and electron-doped (with electrons being the charge carriers) $Nd_{2-x}Ce_xCuO_{4-\delta}$ (16), a large number of works concerning $La_{2-x}A_xCuO_{4-\delta}$ (A = Sr, Ba) (17–19), $Nd_{2-x}Ce_xCuO_{4-\delta}$ (20–31) as well as fluorinated $Nd_2CuO_{4-\delta}$ (32–34), fluorinated $La_{2-x}Sr_xCuO_{4-\delta}$ (35), and fluorinated $Nd_{2-x}Ce_xCuO_{4-\delta}$ (36) have been reported; most of which were focused on the investigation of physical properties such as crystal structure, magnetic nature, electric conductivity, and oxygen nonstoichiometry. The maximal transition temperature has been observed at $x = 0.15$ for $La_{2-x}Sr_xCuO_{4-\delta}$ ($T_c = 40$ K) (19) and for $Nd_{2-x}Ce_xCuO_{4-\delta}$ ($T_c = 24$ K) (16). In recent years, Swamy and co-workers (37, 38) studied the catalytic decomposition of nitrous oxide on hole-doped $La_{2-x}Sr_xCuO_{4-\delta}$ and they attributed the highest activity of $La_{1.85}Sr_{0.15}CuO_4$ to the presence of copper in a mixed oxidation state (Cu^{2+} and Cu^{3+}). After investigating the $La_{2-x}Sr_xCuO_{4-\delta}$ catalysts for CO oxidation reaction, Rajadurai *et al.* (39) concluded that the good catalytic activity could be associated with the positive holes (Cu^{3+}), which may provide a favorable environment for the adsorption of CO and O_2 in CO oxidation. Lee and Ng examined the fluorinated hole-doped $YBa_2Cu_3O_{7-\delta}$ catalysts for the partial oxidation of methane and found that the incorporation of F^- ions enhanced the tendency for the partial oxidation reaction (40). The chemical properties, especially catalytic behaviors of the halogenated superconducting materials, however, have not been well studied. In this paper, we report the catalytic performance of halo-oxide $Ln_{1.85}A_{0.15}CuO_{4-\delta}X_\sigma$ (Ln = La, Nd; A = Sr, Ce; X = F, Cl) as well as $Ln_{1.85}A_{0.15}CuO_{4-\delta}$ (for comparison purposes) for the oxidation of ethane to ethene and characterized these catalysts by means of X-ray diffraction (XRD), X-ray photoelectron spectroscopy (XPS), thermogravimetric analysis (TGA), O_2 temperature-programmed desorption (O_2-TPD), and $^{18}O_2$ isotope-pulsing techniques.

EXPERIMENTAL

The catalysts were prepared by a solid-state reaction method as described in Ref. (16). For $La_{1.85}Sr_{0.15}CuO_{4-\delta}$, the mixtures of La_2O_3, $Sr(NO_3)_2$, and CuO powders (99.9% purities) were well-ground, sintered at 1100°C for 15 h, and annealed at 600°C for 48 h in an oxygen gas flow. For $Nd_{1.85}Ce_{0.15}CuO_{4-\delta}$, the mixtures of Nd_2O_3, CeO_2, and CuO powders (99.9% purities) were well-ground, sintered at 1100°C for 20 h, and slowly cooled to room temperature at a rate of ca. 20°C h^{-1} in air. The fluorination or chlorination of powdered $La_{1.85}Sr_{0.15}CuO_{4-\delta}$ or $Nd_{1.85}Ce_{0.15}CuO_{4-\delta}$ was carried out in a vacuum (ca. 0.1 Torr) furnace first at 350°C for 10 h and then at 660°C for 15 h by using NH_4F or NH_4Cl as halogenating reagent (36). After halogenation, the samples were quenched to room temperature and were in turn ground, tableted, crushed, and sieved to a size range of 80–100 mesh. To make a comparison in XPS studies between Cu ions with different oxidation states, we synthesized the La_4LiCuO_8 (which is well known to contain only Cu^{3+} ions), La_2CuO_4, and Nd_2CuO_4 samples according to the method above. CuO, Nd_2O_3, and CeO_2 were prepared by firing the corresponding oxide powder at 1000°C in air for 5 h and Cu_2O was prepared by calcining fines of Cu metal at 900°C in air for 2 h.

The catalytic performance was measured at atmospheric pressure with 0.5 g of the catalyst and 5.0 g quartz sand being placed in a fixed-bed quartz microreactor (i.d. = 4 mm). The flow rate was 14.8 mL min^{-1} for ethane and 35.2 mL min^{-1} for air, giving a contact time of 1.67×10^{-4} h g mL^{-1} and a $C_2H_6/O_2/N_2$ molar ratio of 2/1/3.7. The product mixture (C_2H_6, C_2H_4, CH_4, CO, and CO_2) was determined online by gas chromatograph (Shimadzu 8A TCD) with Porapak Q and 5A Molecular Sieve being the columns. For the variation of contact time, the reactant flow rate was changed at a fixed catalyst mass (0.5 g). The balances of carbon and oxygen were estimated to be 100 ± 2 and 100 ± 3%, respectively, for every run over the catalysts.

The crystal structures of the catalysts were determined by an X-ray diffractometer (D-MAX, Rigaku) operating at 40 kV and 200 mA using Cu$K\alpha$ radiation. The patterns recorded were referred to the powder diffraction files–PDF-2 Database for the identification of crystal phases. X-ray photoelectron spectroscopy (XPS, VG CLAM 4 MCD analyser) was used to determine the O 1*s*, Ce 3*d*, Nd $3d_{5/2}$, and Cu $2p_{3/2}$ binding energies of surface oxygen, cerium, neodymium, and copper species with Mg$K\alpha$ ($h\nu$ = 1253.6 eV) as the excitation source. The instrumental resolution is 1 eV. Before XPS measurements, the samples were calcined in O_2 (flow rate, 20 mL min^{-1}) at 800°C for 1 h and then cooled in O_2 to room temperature, followed by thermal treatments in He (20 mL min^{-1}) at the desired temperatures for 1 h and then cooling in He to room temperature. The treated samples were then outgassed in the primary vacuum chamber (10^{-5} Torr) for 0.5 h and then introduced into the ultrahigh vacuum chamber (3×10^{-9} Torr) for recording. The C 1*s* line at 284.6 eV was taken as a reference for binding energy calibration. The specific surface areas of the catalysts were measured using a Nova 1200 apparatus.

The TGA experiments were carried out on a thermal analyzer (Shimadzu DT-40) containing an electrobalance. The sample (100 mg) placed in a platinum crucible was kept in a flow of He (20 mL min^{-1}) and heated from room temperature to 800°C at a rate of 10°C min^{-1}. Before performing the TGA experiment, the sample was in turn treated in a He flow of 20 mL min^{-1} at 800°C for 1 h, evacuated *in situ* at the same temperature for 1 h, purged with O_2 (20 mL min^{-1}) for 1 h, and cooled in O_2 to room temperature. Such a

treatment was to guarantee the complete removal of adsorbed CO_2 and H_2O from the sample.

We performed pulse experiments to investigate the reactivity of surface oxygen species. A catalyst sample (0.2 g) was placed in a quartz microreactor and was thermally treated at a desired temperature for 30 min before the pulsing of C_2H_6 or C_2H_6/O_2 (2/1 molar ratio) and the effluent was analyzed on-line by a mass spectrometer (HP G1800A). To confirm the involvement of surface lattice oxygen in the ODE reaction, we treated the sample at a desired temperature in He (flow rate, 20 mL min^{-1}) for 1 h and then kept on pulsing $^{18}O_2$ at a lower temperature until no observable change of pulse size was detected. After purging with He for 0.5 h, we pulsed C_2H_6 or CO onto the treated sample and analyzed the effluent compositions. The pulse size was 65.7 μL (at 25°C, 1 atm) and He (HKO Co., purity >99.995%) was the carrier gas.

The procedures of O_2-TPD experiments as well as the analysis of halogen content were as those described previously (12, 41). The amount of O_2 desorbed from the catalysts was quantified by calibrating the peak areas against a standard pulse of O_2. The oxidation states of copper ions in the superconducting catalysts were determined using the popular titrimetric analysis method described in Ref. (14). The experimental errors for the determination of Cu^{3+} and Cu^+ contents are estimated to be $\pm 0.10\%$.

RESULTS

BET, XRD, and Chemical Analysis Studies

Table 1 summarizes the crystal phases, lattice parameters, compositions, and surface areas of $Ln_{1.85}A_{0.15}CuO_{4-\delta}$ (Ln = La, Nd; A = Sr, Ce) and $Ln_{1.85}A_{0.15}CuO_{4-\delta}X_\sigma$ (X = F, Cl). Based on the halide and Cu^{3+} or Cu^+ contents as well as the assumption of electroneutrality, the value of δ was estimated to be 0.066 for $La_{1.85}Sr_{0.15}CuO_{4-\delta}$ and 0.020 for $Nd_{1.85}Ce_{0.15}CuO_{4-\delta}$, whereas δ and σ values were 0.069 and 0.060 for $La_{1.85}Sr_{0.15}CuO_{4-\delta}F_\sigma$, 0.053 and 0.070 for $La_{1.85}Sr_{0.15}CuO_{4-\delta}Cl_\sigma$, 0.019 and 0.092 for $Nd_{1.85}Ce_{0.15}CuO_{4-\delta}F_\sigma$, and 0.017 and 0.068 for $Nd_{1.85}Ce_{0.15}CuO_{4-\delta}Cl_\sigma$, respectively. By comparing the XRD results with the JCPDS data (Nos. 38-1427, 39-1190, and 39-1390), we deduced that the $La_{1.85}Sr_{0.15}CuO_{3.934}$ and $La_{1.85}Sr_{0.15}CuO_{4-\delta}X_\sigma$ catalysts adopted a tetragonal structure with apical oxygens (T structure), whereas the $Nd_{1.85}Ce_{0.15}CuO_{3.980}$ and $Nd_{1.85}Ce_{0.15}CuO_{4-\delta}X_\sigma$ catalysts adopted a tetragonal structure without apical oxygens (T' structure). The single-phase T or T' structure of the fluorinated or chlorinated materials confirms that the halide ions were incorporated into the $Ln_{1.85}A_{0.15}CuO_{4-\delta}$ lattice. Although the introduction of halide ions in limited amount did not induce any phase transformation and any significant change in surface area, there were changes in lattice parameters; the intercalation of halide ions brought about the enlargement of the Sr-substituted cuprate lattices and the shrinkage of the Ce-substituted cuprate lattices. From Table 1, one can realize that the doping of halide ions has caused (i) the Cu^{3+} content in $La_{1.85}Sr_{0.15}CuO_{4-\delta}$ to rise, (ii) the Cu^+ content in $Nd_{1.85}Ce_{0.15}CuO_{4-\delta}$ to fall, and (iii) the oxygen vacancy density in both catalyst series to decrease. After 60 h of on-stream reaction at 660°C or O_2-TPD (from 25 to 800°C), the halogen contents remained unaltered. It should be noted that according to the results of titration experiments, there were no Cu^+ ions in the Sr-doped samples and no Cu^{3+} ions in the Ce-doped samples.

TABLE 1

Physical Properties of $Ln_{1.85}A_{0.15}CuO_{4-\delta}$ and $Ln_{1.85}A_{0.15}CuO_{4-\delta}X_\sigma$ Catalysts

Catalyst	Crystal phase[a]	Lattice parameter[b] (Å)			Cu^{3+} or Cu^{+c} (mol%)	F or Cl content (wt%)	δ	σ	Surface area ($m^2\ g^{-1}$)
		a	b	c					
$La_{1.85}Sr_{0.15}CuO_{4-\delta}$	T structure	3.775	3.775	13.236	1.8	—	0.066	—	2.04
$La_{1.85}Sr_{0.15}CuO_{4-\delta}F_\sigma$	T structure	3.781	3.781	13.240	7.2	0.29	0.069	0.060	1.92
$La_{1.85}Sr_{0.15}CuO_{4-\delta}Cl_\sigma$	T structure	3.787	3.787	13.249	6.4	0.47 (0.45)[d] [0.46][e]	0.070	0.053	1.97
$Nd_{1.85}Ce_{0.15}CuO_{4-\delta}$	T' structure	3.948	3.948	12.089	15.4[f]	—	0.030	—	2.02
$Nd_{1.85}Ce_{0.15}CuO_{4-\delta}F_\sigma$	T' structure	3.957	3.957	12.063	9.6[f]	0.45 (0.46)[d] [0.44][e]	0.019	0.092	1.98
$Nd_{1.85}Ce_{0.15}CuO_{4-\delta}Cl_\sigma$	T' structure	3.961	3.961	12.074	11.5[f]	0.62	0.017	0.068	1.95

[a] T or T' denotes tetragonal structure. The only difference between T and T' structures is that there are no apical oxygen atoms in the T' structure.
[b] Calculated according to the least-squares refinement method which was supposed to fit the tetragonal symmetry.
[c] Calculated according to the assumption that there are only Cu^{3+} and Cu^{2+} ions in the Sr-doped catalysts or Cu^{2+} and Cu^+ ions in the Ce-doped catalysts.
[d] Data in parentheses were obtained after 60 h of on-stream ODE reaction.
[e] Data in square brackets were obtained after O_2-TPD.
[f] Cu^+ contents.

Catalytic Activity

One of our previous studies indicates that quartz sand is poor in catalytic activity at 680°C (14). Figure 1 shows the catalytic performance of $Ln_{1.85}A_{0.15}CuO_{4-\delta}$ and $Ln_{1.85}A_{0.15}CuO_{4-\delta}X_{\sigma}$. With the rise in temperature from 500 to 680°C over the two halide-free $Ln_{1.85}A_{0.15}CuO_{4-\delta}$ catalysts (Figs. 1a and 1b), C_2H_6 conversion, C_2H_4 selectivity, and C_2H_4 yield increased, whereas CO_x selectivity decreased; O_2 conversions were close to 100% and CH_4 selectivities were 0%; the best activity (49.9% C_2H_6 conversion, 30.3% C_2H_4 selectivity, and 15.1% C_2H_4 yield over $La_{1.85}Sr_{0.15}CuO_{3.934}$, and 40.6% C_2H_6 conversion, 29.8% C_2H_4 selectivity, and 12.1% C_2H_4 yield over $Nd_{1.85}Ce_{0.15}CuO_{3.980}$) was observed at 680°C. Over $La_{1.85}Sr_{0.15}CuO_{4-\delta}X_{\sigma}$ (Figs. 1c and 1e), with the increase in temperature, C_2H_6 and O_2 conversions, CH_4 selectivity, and C_2H_4 yield increased; C_2H_4 selectivity reached a maximum value at 660°C, whereas CO_x selectivity came to a minimum value; at 660°C, C_2H_4 yield reached a maximum value of 56.9% over $La_{1.85}Sr_{0.15}CuO_{3.931}F_{0.060}$ and 60.6% over $La_{1.85}Sr_{0.15}CuO_{3.930}Cl_{0.053}$. Over the $Nd_{1.85}Ce_{0.15}CuO_{4-\delta}X_{\sigma}$ catalyst (Figs. 1d and 1f), with the rise in temperature from 500 to 680°C, C_2H_6 and O_2 conversions, C_2H_4 yield, and CH_4 selectivity augmented (CO_x selectivity decreased); C_2H_4 selectivity reached a maximum value of 61.8% over $Nd_{1.85}Ce_{0.15}CuO_{3.981}F_{0.092}$ and 58.2% over $Nd_{1.85}Ce_{0.15}CuO_{3.983}Cl_{0.068}$ at 660°C; C_2H_4 yield reached a maximum value of 44.6% over the former and 38.3% over the latter. Compared to $Ln_{1.85}A_{0.15}CuO_{4-\delta}$, the halide-doped catalysts showed much higher C_2H_4 selectivities at lower C_2H_6 conversion (<40%) levels (Fig. 1).

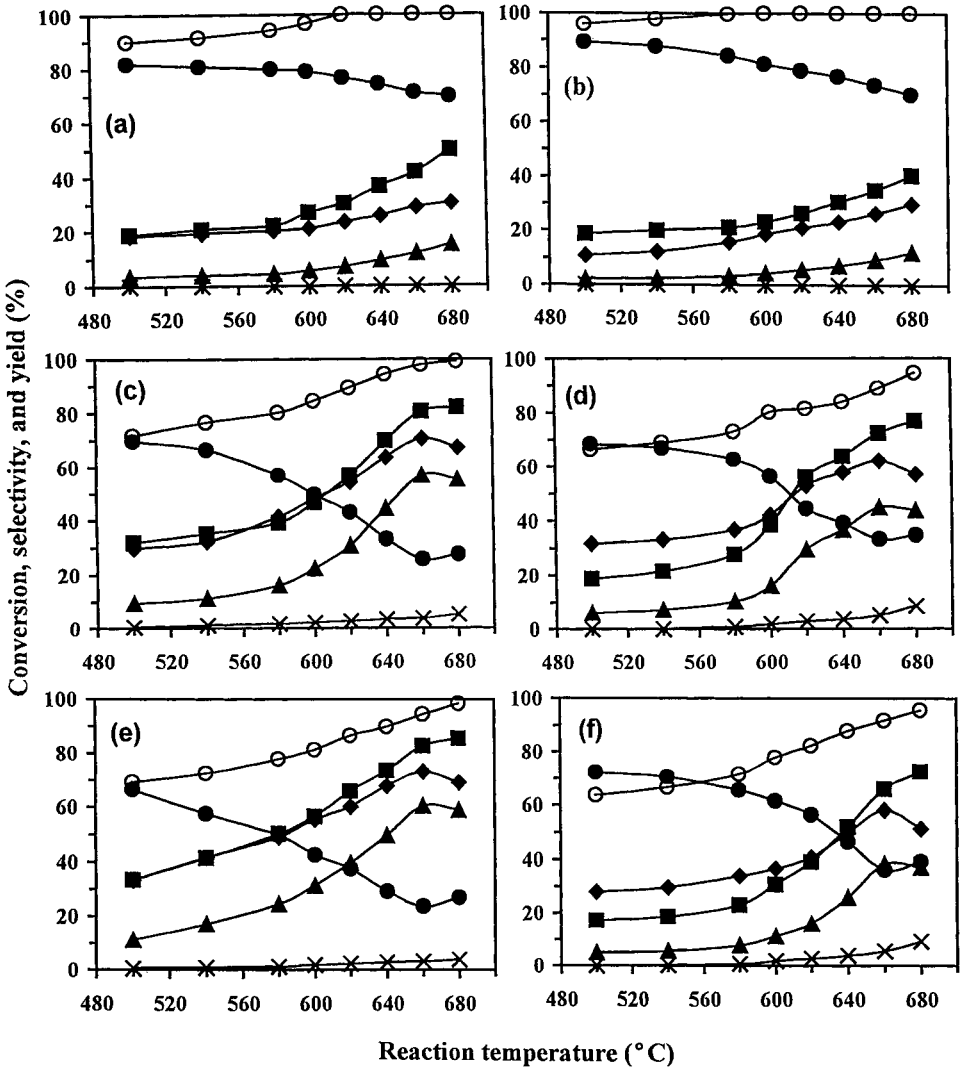

FIG. 1. Catalytic performance of (a) $La_{1.85}Sr_{0.15}CuO_{3.934}$, (b) $Nd_{1.85}Ce_{0.15}CuO_{3.980}$, (c) $La_{1.85}Sr_{0.15}CuO_{3.931}F_{0.060}$, (d) $Nd_{1.85}Ce_{0.15}CuO_{3.981}F_{0.092}$, (e) $La_{1.85}Sr_{0.15}CuO_{3.930}Cl_{0.053}$, and (f) $Nd_{1.85}Ce_{0.15}CuO_{3.983}Cl_{0.068}$ as related to reaction temperature. (■) C_2H_6 conversion, (◆) C_2H_4 selectivity, (▲) C_2H_4 yield, (○) O_2 conversion, (●) CO_x ($CO + CO_2$) selectivity, and (×) CH_4 selectivity.

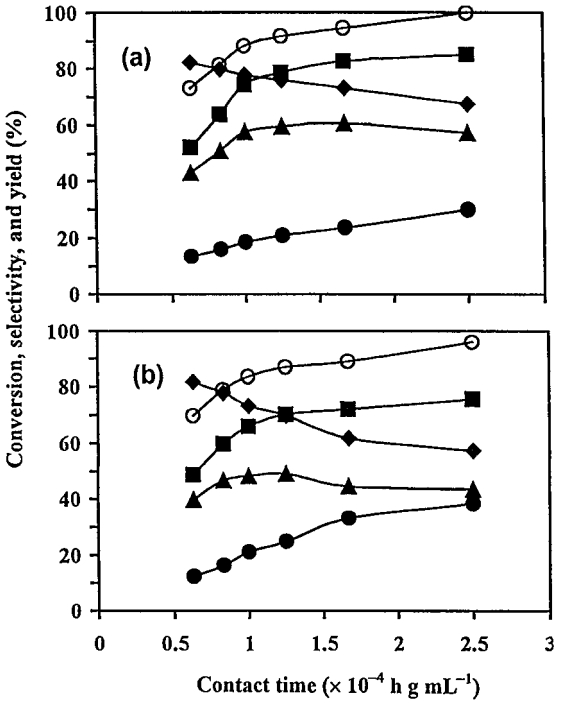

FIG. 2. Catalytic performance of (a) $La_{1.85}Sr_{0.15}CuO_{3.930}Cl_{0.053}$ and (b) $Nd_{1.85}Ce_{0.15}CuO_{3.981}F_{0.092}$ as related to contact time at 660°C. (■) C_2H_6 conversion, (◆) C_2H_4 selectivity, (▲) C_2H_4 yield, (○) O_2 conversion, and (●) CO_x selectivity.

In the lifetime studies, we performed the on-stream ODE reaction at 660°C and 1.67×10^{-4} h g mL^{-1} for 60 h over $La_{1.85}Sr_{0.15}CuO_{3.930}Cl_{0.053}$ and $Nd_{1.85}Ce_{0.15}CuO_{3.981}F_{0.092}$. The results indicated that the performance of the two catalysts was stable (the fluctuations in C_2H_4 conversion and C_2H_4 selectivity were below 3%); i.e., they were durable within a period of 60 h.

The catalytic performance of $La_{1.85}Sr_{0.15}CuO_{3.930}Cl_{0.053}$ and $Nd_{1.85}Ce_{0.15}CuO_{3.981}F_{0.092}$ as related to contact time at 660°C is shown in Fig. 2. With the prolongation in contact time from 0.63×10^{-4} to 2.50×10^{-4} h g mL^{-1} over the Sr-doped catalyst (Fig. 2a), C_2H_6 and O_2 conversions and CO_x selectivity increased from 52.1, 72.9, and 13.4% to 85.1, 99.8, and 29.9%, respectively; C_2H_4 selectivity decreased from 82.3 to 67.4% whereas C_2H_4 yield reached a maximum value of 60.6% at a contact time of 1.67×10^{-4} h g mL^{-1}. Over the Ce-doped catalyst (Fig. 2b), C_2H_6 and O_2 conversions and CO_x selectivity increased from 48.6, 69.7, and 12.3% to 75.6, 95.8, and 38.5%, respectively; C_2H_4 selectivity decreased from 81.6 to 57.3% whereas C_2H_4 yield reached a maximum value of 49.0% at a contact time of 1.25×10^{-4} h g mL^{-1}. Similar results were obtained when the two catalysts were well dispersed in quartz sand.

To investigate the reactivity of C_2H_4 toward O_2 over $La_{1.85}Sr_{0.15}CuO_{3.934}$, $Nd_{1.85}Ce_{0.15}CuO_{3.980}$, $La_{1.85}Sr_{0.15}CuO_{3.930}Cl_{0.053}$, and $Nd_{1.85}Ce_{0.15}CuO_{3.981}F_{0.092}$, we carried out C_2H_4 oxidation experiments under reaction conditions similar to those adopted in C_2H_6 oxidation reaction at 660°C, and the results as well as those of C_2H_6 oxidation reactions are listed in Table 2. One can observe that the C_2H_4 conversion was 14.6% over the Cl-doped catalyst and 12.4% over the F-doped catalyst whereas it was 35.2% over $La_{1.85}Sr_{0.15}CuO_{3.934}$ and 29.7% over $Nd_{1.85}Ce_{0.15}CuO_{3.980}$. Furthermore, the CO/CO_2 ratios in the product mixture over the halide-doped catalysts were much higher than that over the halogen-free catalysts.

XPS Studies

Figure 3 illustrates the Ce 3*d* and Nd $3d_{5/2}$ spectra of CeO_2, Nd_2O_3, Nd_2CuO_4, $Nd_{1.85}Ce_{0.15}CuO_{3.980}$, and $Nd_{1.85}Ce_{0.15}CuO_{3.981}F_{0.092}$ samples which were treated in He at 25°C for 1 h, respectively. It can be observed from Fig. 3I that the Nd $3d_{5/2}$ core-level spectra of Nd_2CuO_4, $Nd_{1.85}Ce_{0.15}CuO_{3.980}$, and $Nd_{1.85}Ce_{0.15}CuO_{3.981}F_{0.092}$ are rather similar to that of Nd_2O_3; the component at ca. 982 eV (binding energy) can be ascribed to a $4f^3$ feature and the one at ca. 972 eV to a $4f^4\underline{L}$ ($\underline{L}$ denotes a ligand hole) feature (42). These results indicate that the Nd in the Ce-doped cuprate catalysts is in a formal trivalent oxidation state. From Fig. 3II, one can realize that the spectra of the three Ce-doped cuprates show a characteristic triple-peak structure.

TABLE 2

Catalytic Performance of $Ln_{1.85}A_{0.15}CuO_{4-\delta}$ and $Ln_{1.85}A_{0.15}CuO_{4-\delta}X_{\sigma}$ Catalysts for the Oxidation of Ethane and Ethene at 660°C and 1.67×10^{-4} h g mL^{-1}

	Oxidation of C_2H_4[a]			Oxidation of C_2H_6		
Catalyst	C_2H_4 conversion (%)	CO/CO_2 ratio	Rate of C_2H_4 reaction (10^{18} molecules m^{-2} s^{-1})	C_2H_6 conversion (%)	C_2H_4 selectivity (%)	Rate of C_2H_6 reaction (10^{18} molecules m^{-2} s^{-1})
$La_{1.85}Sr_{0.15}CuO_{3.934}$	35.2	1/27.5	0.343	41.8	28.8	0.407
$Nd_{1.85}Ce_{0.15}CuO_{3.980}$	29.7	1/29.4	0.292	34.9	26.3	0.324
$La_{1.85}Sr_{0.15}CuO_{3.930}Cl_{0.053}$	14.6	1/5.3	0.147	82.8	73.2	0.835
$Nd_{1.85}Ce_{0.15}CuO_{3.981}F_{0.092}$	12.4	1/4.2	0.125	72.1	61.8	0.724

[a] At $C_2H_4/O_2/N_2$ molar ratio = 2/1/3.7.

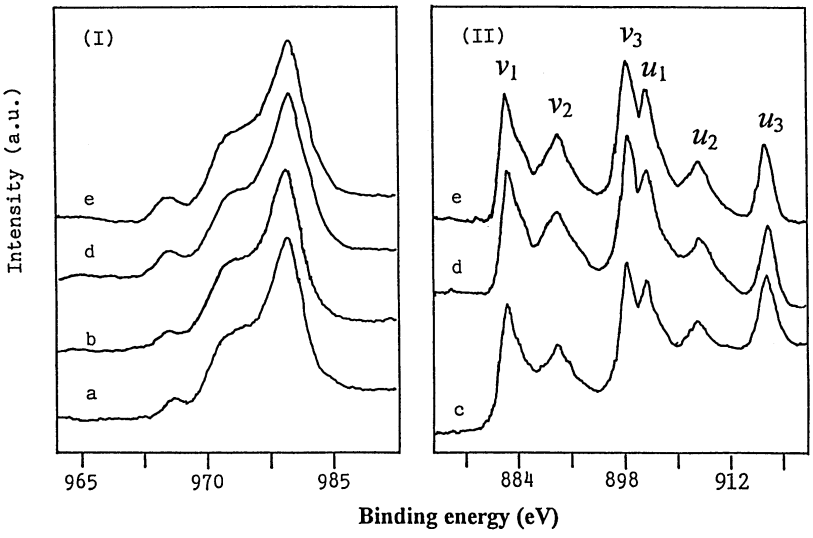

FIG. 3. (I) Nd $3d_{5/2}$ and (II) Ce $3d_{3/2}$ spectra: (a) Nd_2O_3, (b) Nd_2CuO_4, (c) CeO_2, (d) $Nd_{1.85}Ce_{0.15}CuO_{3.980}$, and (e) $Nd_{1.85}Ce_{0.15}CuO_{3.981}F_{0.092}$ samples treated in He at 25°C for 1 h.

Two sets of the three peaks denoted by (v_1, v_2, v_3) and (u_1, u_2, u_3) can be ascribed to $3d_{5/2}$ and $3d_{3/2}$, respectively. By comparing the Ce 3*d* spectra of CeO_2 (Ce oxidation state, +4) and Ce_2O_3 (Ce oxidation state, +3) (43), one can see that the spectra of the Ce-containing cuprates are quite similar to that of CeO_2 but different from that of Ce_2O_3, indicating that the Ce ions exist in an oxidation state of +4 in the Ce-substituted catalysts.

For comparison purposes, the Cu $2p_{3/2}$ spectra of Cu_2O, CuO, Nd_2CuO_4, La_2CuO_4, and La_4LiCuO_8 recorded after treatment in He at 25°C are compiled together in Fig. 4. There is only one peak at 932.0 eV for Cu_2O (Fig. 4a) and at 934.6 eV for La_4LiCuO_8 (Fig. 4e), corresponding to the signals due to Cu^+ (44) and Cu^{3+} (45). The Cu $2p_{3/2}$ spectra of CuO (Fig. 4b), Nd_2CuO_4 (Fig. 4c), and La_2CuO_4 (Fig. 4d) were rather similar: there are a main peak at ca. 933 eV and shake-up satellite features in the binding energy range of 940–945 eV; these signals are characteristics of Cu^{2+} ions (44). We did not detect any signal that could be assigned to Cu^{3+} ions in La_2CuO_4. Figure 5 shows the Cu $2p_{3/2}$ spectra of the $Ln_{1.85}A_{0.15}CuO_{4-\delta}$ and $Ln_{1.85}A_{0.15}CuO_{4-\delta}X_\sigma$ samples that had been treated in He at various temperatures, respectively. For the $La_{1.85}Sr_{0.15}CuO_{3.934}$ sample treated at 25°C, there is a peak at 933.6 eV with a shoulder at 934.6 eV (Fig. 5Ia); with the rise in treatment temperature (from 25 to 700°C), the shoulder peak decreased in intensity and disappeared at 700°C; signal intensities of the shake-up satellite within the region of 940–945 eV increased (Figs. 5Ia–Ic). For $Nd_{1.85}Ce_{0.15}CuO_{3.980}$, with the rise in treatment temperature from 25 to 700°C (Figs. 5IIa–IIc), the intensities of the satellite signals decreased, whereas the shoulder signal (at 932.7 eV) of the main peak (at 933.6 eV) increased in intensity. We assign the signal at ca. 934.6 eV to Cu^{3+}, the one at ca. 933.6 eV to Cu^{2+}, and the one at ca. 932.7 eV to Cu^+. For the Cl-containing $La_{1.85}Sr_{0.15}CuO_{3.930}Cl_{0.053}$ samples, the nature of Cu species and the features of the Cu $2p_{3/2}$ spectra (Figs. 5IIIa–IIIc) are rather similar to those of the Cl-free Sr-doped samples; only the intensity of the Cu^{3+} signal in the former is stronger than that in the latter, respectively. Similarly, the variation trend of the Cu $2p_{3/2}$ spectra of $Nd_{1.85}Ce_{0.15}CuO_{3.981}F_{0.092}$ from 25 to 700°C (Figs. 5IVa–IVc) resembles that of the F-free Ce-doped samples, except that the intensity of the Cu^+ signal of the former is stronger than that of the latter.

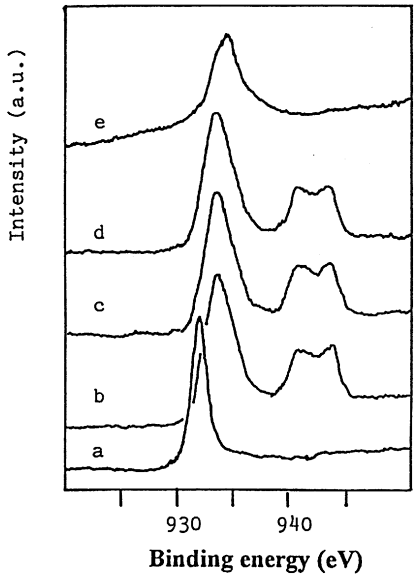

FIG. 4. Cu $2p_{3/2}$ spectra of (a) Cu_2O, (b) CuO, (c) Nd_2CuO_4, (d) La_2CuO_4, and (e) La_4LiCuO_8 samples treated in He at 25°C for 1 h.

Table 3 lists the changes in intensity ratio (I_s/I_m) of the shake-up satellite (due to Cu^{2+}) and the Cu $2p_{3/2}$ main peak

TABLE 3

The Changes in Relative Intensity (I_s/I_m) of the Shake-Up Satellite and the Main Cu $2p_{3/2}$ Peak of $La_{1.85}Sr_{0.15}CuO_{3.934}$, $Nd_{1.85}Ce_{0.15}CuO_{3.980}$, $La_{1.85}Sr_{0.15}CuO_{3.930}Cl_{0.053}$, and $Nd_{1.85}Ce_{0.15}CuO_{3.981}F_{0.092}$ after Thermal Treatments in He at Various Temperatures

Catalyst	I_s/I_m			
	Treatment temperature (°C)			
	25	490[a]	600	700
$La_{1.85}Sr_{0.15}CuO_{3.934}$	0.35	0.37	0.38	0.39
$Nd_{1.85}Ce_{0.15}CuO_{3.980}$	0.25	0.26	0.24	0.23
$La_{1.85}Sr_{0.15}CuO_{3.930}Cl_{0.053}$	0.31	0.32	0.33	0.36
$Nd_{1.85}Ce_{0.15}CuO_{3.981}F_{0.092}$	0.27	0.26	0.25	0.21

[a] 490°C for $La_{1.85}Sr_{0.15}CuO_{3.934}$, 480°C for $Nd_{1.85}Ce_{0.15}CuO_{3.980}$, and 550°C for $La_{1.85}Sr_{0.15}CuO_{3.930}Cl_{0.053}$ and $Nd_{1.85}Ce_{0.15}CuO_{3.981}F_{0.092}$.

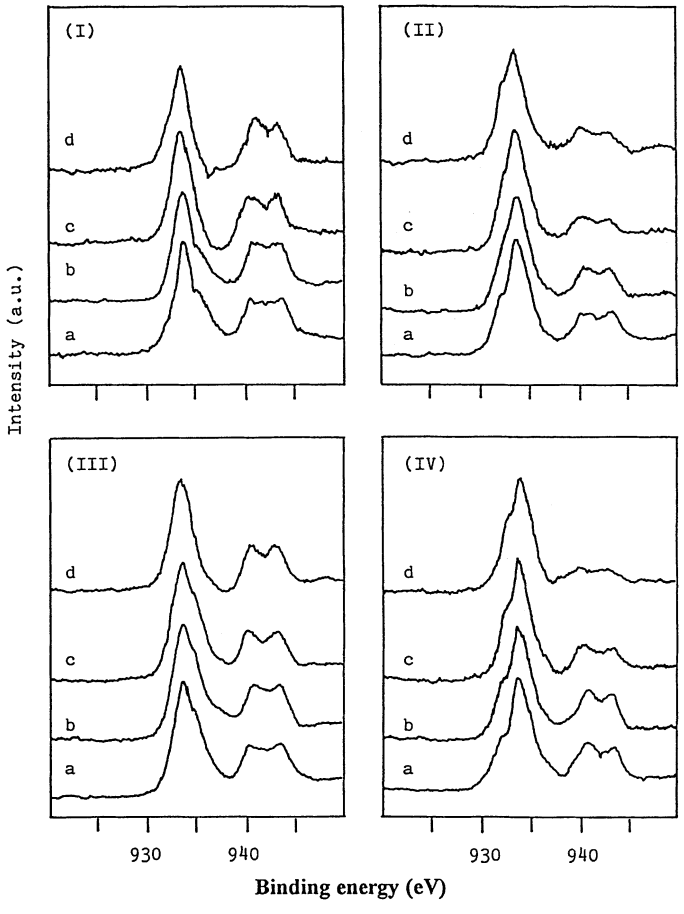

FIG. 5. Cu $2p_{3/2}$ spectra of (I) $La_{1.85}Sr_{0.15}CuO_{3.934}$, (II) $Nd_{1.85}Ce_{0.15}CuO_{3.980}$, (III) $La_{1.85}Sr_{0.15}CuO_{3.930}Cl_{0.053}$, and (IV) $Nd_{1.85}Ce_{0.15}CuO_{3.981}F_{0.092}$ after treatment in He for 0.5 h: (a) at 25°C, (b) at 490°C for $La_{1.85}Sr_{0.15}CuO_{3.934}$, at 480°C for $Nd_{1.85}Ce_{0.15}CuO_{3.980}$, and at 550°C for $La_{1.85}Sr_{0.15}CuO_{3.930}Cl_{0.053}$ and $Nd_{1.85}Ce_{0.15}CuO_{3.981}F_{0.092}$, (c) at 600°C, and (d) at 700°C.

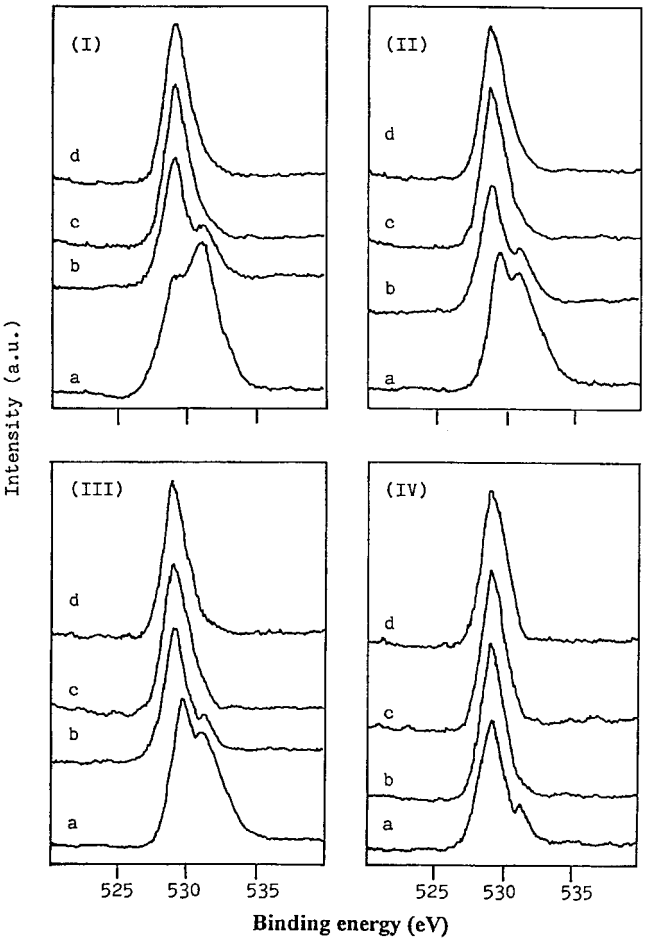

FIG. 6. O 1*s* spectra of (I) $La_{1.85}Sr_{0.15}CuO_{3.934}$, (II) $Nd_{1.85}Ce_{0.15}CuO_{3.980}$, (III) $La_{1.85}Sr_{0.15}CuO_{3.930}Cl_{0.053}$, and (IV) $Nd_{1.85}Ce_{0.15}CuO_{3.981}F_{0.092}$ after treatment in He for 0.5 h: (a) at 25°C, (b) at 490°C for $La_{1.85}Sr_{0.15}CuO_{3.934}$, at 480°C for $Nd_{1.85}Ce_{0.15}CuO_{3.980}$, and at 550°C for $La_{1.85}Sr_{0.15}CuO_{3.930}Cl_{0.053}$ and $Nd_{1.85}Ce_{0.15}CuO_{3.981}F_{0.092}$, (c) at 600°C, and (d) at 700°C.

in Fig. 5. With the rise in treatment temperature, the I_s/I_m ratio increased for the Sr-doped samples, indicating the increase in Cu^{2+} concentration. As for the Ce-doped samples, the value of I_s/I_m declined, indicating a drop in Cu^{2+} content.

Shown in Fig. 6 are the O 1*s* spectra of the $Ln_{1.85}A_{0.15}CuO_{4-\delta}$ and $Ln_{1.85}A_{0.15}O_{4-\delta}X_{\sigma}$ samples treated in He at different temperatures, respectively. After treatment in He at 25°C, there are two O 1s peaks at 528.7 and 531.4 eV for $La_{1.85}Sr_{0.15}CuO_{3.934}$ (Fig. 6Ia), at 528.9 and 531.2 eV for $Nd_{1.85}Ce_{0.15}CuO_{3.980}$ (Fig. 6IIa), at 529.8 and 531.3 eV for $La_{1.85}Sr_{0.15}CuO_{3.930}Cl_{0.053}$ (Fig. 6IIIa), and at 529.6 and 531.5 eV for $Nd_{1.85}Ce_{0.15}CuO_{3.981}F_{0.092}$ (Fig. 6IVa). We assign the signal at lower binding energy (528.7–529.8 eV) to surface lattice oxygen and the one at higher binding energy (531.2–531.5 eV) to adsorbed oxygen species such as O^- or OH^- (46–49). When the treatment temperature was raised to the 480–550°C range, the signal due to adsorbed oxygen

TABLE 4

TGA Results of $Ln_{1.85}A_{0.15}CuO_{4-\delta}$ and $Ln_{1.85}A_{0.15}CuO_{4-\delta}X_{\sigma}$ Catalysts

Catalyst	Experimental weight loss (wt%)		Theoretical weight loss[a] (wt%)	
	<600°C	600–800°C	<600°C	600–800°C
$La_{1.85}Sr_{0.15}CuO_{3.934}$	0.23	0.03	0.27	2.02
$Nd_{1.85}Ce_{0.15}CuO_{3.980}$	0.11	0.02	0.08	1.63
$La_{1.85}Sr_{0.15}CuO_{3.930}Cl_{0.053}$	0.09	0.12	0.07	0.09
$Nd_{1.85}Ce_{0.15}CuO_{3.981}F_{0.092}$	0.02	0.14	0	1.73

[a] Calculations based on the desorption of the oxygen adsorbed at oxygen vacancies below 600°C ($2Cu^{3+} + 2O^{-}_{vacancy} \rightarrow 2Cu^{2+} + O_2$ for Sr-doped catalysts and $2Cu^{2+} + 2O^{-}_{vacancy} \rightarrow 2Cu^{+} + O_2$ for Ce-doped catalysts) and the desorption due to partial reduction of Cu ions between 600 and 800°C ($2Cu^{3+} + O^{2-}_{lattice} \rightarrow 2Cu^{2+} + 1/2O_2$ for Sr-doped catalysts and $2Cu^{2+} + O^{2-}_{lattice} \rightarrow 2Cu^{+} + 1/2O_2$ for Ce-doped catalysts).

species decreased in intensity (Figs. 6Ib–IVb). After treatments in He at 600 and 700°C, there is only one O 1*s* peak at ca. 529 eV for the $La_{1.85}Sr_{0.15}CuO_{3.934}$ (Figs. 6Ic and 6Id) and $Nd_{1.85}Ce_{0.15}CuO_{3.980}$ samples (Figs. 6IIc and 6IId) and only one O 1*s* peak at ca. 530 eV for the $La_{1.85}Sr_{0.15}CuO_{3.930}Cl_{0.053}$ (Figs. 6IIIc and 6IIId) and $Nd_{1.85}Ce_{0.15}CuO_{3.981}F_{0.092}$ samples (Figs. 6IVc and 6IVd); these peaks could be assigned to surface lattice oxygen (44, 46–49). One can also observe that with the rise in treatment temperature, the component at ca. 531 eV decreases markedly in intensity and disappeared at 600°C whereas the intensity of the component at 529–530 eV increases (Figs. 6I–IV).

TGA, O_2-TPD, and Pulsing Studies

The TGA results obtained over $Ln_{1.85}A_{0.15}CuO_{4-\delta}$, $La_{1.85}Sr_{0.15}CuO_{3.930}Cl_{0.053}$, and $Nd_{1.85}Ce_{0.15}CuO_{3.981}F_{0.092}$ are summarized in Table 4. There were weight losses below 600°C and between 600 and 800°C. The weight loss below 600°C was due to the desorption of oxygen located at oxygen vacancies and that between 600 and 800°C was due to the reduction of a certain amount of Cu^{3+} to Cu^{2+} or Cu^{2+} to Cu^{+}. Below 600°C, the experimental values were rather close to the theoretical ones, whereas between 600 and 800°C, the former were less than the latter, except for $La_{1.85}Sr_{0.15}CuO_{3.930}Cl_{0.053}$.

We conducted $^{18}O_2$, C_2H_6, and CO pulsing experiments over $La_{1.85}Sr_{0.15}CuO_{3.930}Cl_{0.053}$ and $Nd_{1.85}Ce_{0.15}CuO_{3.981}F_{0.092}$ which had been treated under various conditions. In the case of pulsing C_2H_6 over the $^{18}O_2$-treated catalysts, besides the signals due to C_2H_6 and C_2H_4, we detected signals at $m/e = 20$, 19, and 18, corresponding to $H_2{}^{18}O$, ^{18}OH, and ^{18}O, respectively, indicating that surface lattice $^{18}O^{2-}$ (incorporated in the $Ln_{1.85}A_{0.15}O_{4-\delta}X_{\sigma}$ lattice by $^{18}O/^{16}O$ exchange during $^{18}O_2$-pulsing) had reacted with C_2H_6. In the case of CO pulsing, besides the signals of CO, we detected a signal with $m/e = 46$, corresponding to CO ^{18}O; the results indicate the involvement of lattice ^{18}O in the oxidation of CO.

Summarized in Table 5 are the changes in copper oxidation state and catalytic performance of $Ln_{1.85}A_{0.15}CuO_{4-\delta}$, $La_{1.85}Sr_{0.15}CuO_{3.930}Cl_{0.053}$, and $Nd_{1.85}Ce_{0.15}CuO_{3.981}F_{0.092}$ treated under various conditions. With a rise in temperature from 480 to 700°C in a He atmosphere, the Cu^{3+} contents

TABLE 5

The Changes in Cu^{3+} or Cu^{+} Content and Catalytic Performance of $La_{1.85}Sr_{0.15}CuO_{3.934}$, $Nd_{1.85}Ce_{0.15}CuO_{3.980}$, $La_{1.85}Sr_{0.15}CuO_{3.930}Cl_{0.053}$, and $Nd_{1.85}Ce_{0.15}CuO_{3.981}F_{0.092}$ in a C_2H_6 or C_2H_6/O_2 Pulse after Thermal Treatment in He at Different Temperatures for 0.5 h, Respectively

Catalyst	490°C[a]			600°C			700°C		
	Cu^{3+} or Cu^{+b} content (mol%)	C_2H_6 conversion (%)	C_2H_4 selectivity (%)	Cu^{3+} or Cu^{+b} content (mol%)	C_2H_6 conversion (%)	C_2H_4 selectivity (%)	Cu^{3+} or Cu^{+b} content (mol%)	C_2H_6 conversion (%)	C_2H_4 selectivity (%)
$La_{1.85}Sr_{0.15}CuO_{3.934}$	0.8	16.4[c]	18.2	0.3	29.7	29.6	0.1	53.6	55.4
	[1.5]	(15.6)[d]	(16.7)	[1.7]	(27.2)	(22.6)	[1.9]	(52.3)	(38.7)
$Nd_{1.85}Ce_{0.15}CuO_{3.980}$	15.7	18.2	9.9	16.9	26.5	25.8	17.2	51.4	50.7
	[15.2]	(17.3)	(8.8)	[14.8]	(24.7)	(23.2)	[15.5]	(49.2)	(36.3)
$La_{1.85}Sr_{0.15}CuO_{3.930}Cl_{0.053}$	5.3	43.8	43.4	4.5	65.3	62.4	0.2	92.6	84.7
	[6.5]	(42.7)	(44.1)	[6.6]	(57.6)	(57.1)	[6.8]	(89.2)	(64.5)
$Nd_{1.85}Ce_{0.15}CuO_{3.981}F_{0.092}$	10.0	24.2	35.1	10.3	62.1	57.2	16.1	85.4	79.8
	[9.5]	(23.3)	(34.7)	[9.4]	(57.2)	(53.6)	[9.2]	(80.5)	(53.2)

[a] Temperature for thermal treatment and reactant pulsing: 490°C for $La_{1.85}Sr_{0.15}CuO_{3.934}$, 480°C for $Nd_{1.85}Ce_{0.15}CuO_{3.980}$, and 550°C for $La_{1.85}Sr_{0.15}CuO_{3.930}Cl_{0.053}$ and $Nd_{1.85}Ce_{0.15}CuO_{3.981}F_{0.092}$.

[b] Cu^{3+} contents for the Sr-doped catalysts or Cu^{+} contents for the Ce-doped catalysts after thermal treatments in He at temperatures varied from 480 to 700°C, respectively. Data in square brackets were obtained after the thermally treated sample was exposed to an O_2 flow (20 mL min^{-1}) at the same temperature for 0.5 h.

[c] In a pulse of C_2H_6.

[d] Values in parentheses were obtained in a pulse of C_2H_6/O_2 (molar ratio = 2/1).

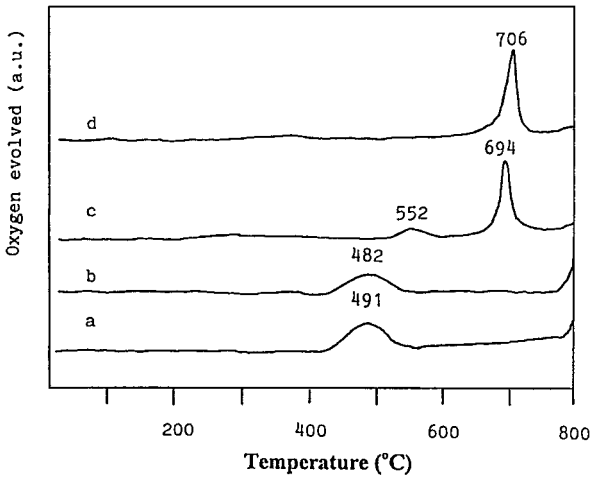

FIG. 7. O_2-TPD profiles of (a) $La_{1.85}Sr_{0.15}CuO_{3.934}$, (b) $Nd_{1.85}Ce_{0.15}CuO_{3.980}$, (c) $La_{1.85}Sr_{0.15}CuO_{3.930}Cl_{0.053}$, and (d) $Nd_{1.85}Ce_{0.15}CuO_{3.981}F_{0.092}$.

decreased for the Sr-doped catalysts and the Cu^+ contents increased for the Ce-doped catalysts. Exposing the treated samples to an O_2 flow at the same temperature for 0.5 h would result in the restoration of the Cu^{3+} or Cu^+ contents. When subjected to a pulse of C_2H_6 or C_2H_6/O_2 (molar ratio = 2/1), the thermally treated $La_{1.85}Sr_{0.15}CuO_{3.934}$, $Nd_{1.85}Ce_{0.15}CuO_{3.980}$, and $La_{1.85}Sr_{0.15}CuO_{3.930}Cl_{0.053}$, and $Nd_{1.85}Ce_{0.15}CuO_{3.981}F_{0.092}$ catalysts showed C_2H_4 selectivity and C_2H_6 conversion noticeably higher than the untreated one, especially when the treatment temperatures were above 600°C. Below 600°C, each catalyst gave similar C_2H_4 selectivity and C_2H_6 conversion either in a pulse of C_2H_6 or in a pulse of C_2H_6/O_2.

Figure 7 shows the O_2-TPD profiles of $Ln_{1.85}A_{0.15}CuO_{4-\delta}$, $La_{1.85}Sr_{0.15}CuO_{3.930}Cl_{0.053}$, and $Nd_{1.85}Ce_{0.15}CuO_{3.981}F_{0.092}$. For the halogen-free catalysts, a broad peak appears at ca. 491°C (amount to 67.4 μmol g^{-1} of O_2 desorption) and a peak begins at ca. 790°C for $La_{1.85}Sr_{0.15}CuO_{3.934}$ (Fig. 7a), and a broad peak at ca. 482°C (amount to 33.3 μmol g^{-1} of O_2 desorption) and a peak starts at ca. 775°C for $Nd_{1.85}Ce_{0.15}CuO_{3.980}$ (Fig. 7b). For $La_{1.85}Sr_{0.15}CuO_{3.930}Cl_{0.053}$ (Fig. 7c), there are a weak desorption peak at ca. 552°C and a strong one at ca. 694°C, corresponding to 25.4 and 35.2 μmol g^{-1} of O_2 desorption, respectively. Only one peak at ca. 706°C is observed for the F-incorporated Ce-doped catalyst (Fig. 7d) and the O_2 desorption amount is 39.6 μmol g^{-1}.

DISCUSSION

Enhanced Catalytic Performance by Halogen Incorporation

Simultaneous increase in reactant conversion and product selectivity is unusual in heterogeneous catalysis. In C_2H_6 oxidation at a particular O_2 conversion, C_2H_4 selectivity and C_2H_6 conversion can augment simultaneously if deep oxidation is reduced or suppressed. From Figs. 1a–1f, one can observe that with the intercalation of halide ions into the $Ln_{1.85}A_{0.15}CuO_{4-\delta}$ lattice, C_2H_6 conversion and C_2H_4 selectivity increased remarkably. Usually, a comparison of C_2H_4 selectivities between various catalysts should be based on a similar level of C_2H_6 conversion. It is difficult, however, to make such a comparison here because at a particular C_2H_6 conversion, the reaction temperature and O_2 conversion varied markedly from catalyst to catalyst. Hence, we chose to compare the C_2H_4 selectivities and C_2H_6 conversions of the catalysts under similar reaction conditions (for example, at 660°C and at ca. 90% O_2 conversion). As pointed out by Shi *et al.* (50), C_2H_4 was the major carbon source for CO_x formation at or above 650°C in ODE reactions. If C_2H_4 deep oxidation was reduced or suppressed, C_2H_4 selectivity would be enhanced. The significant drop in C_2H_4 conversion in C_2H_4 oxidation reaction (Table 2) and the obvious rise in C_2H_4 selectivity in the ODE reaction (Figs. 1c–1f and Table 2) indicate that the doping of F^- or Cl^- ions to $Ln_{1.85}A_{0.15}CuO_{4-\delta}$ could reduce the deep oxidation of C_2H_4. It should be noted that the possible roles of gas-phase chemistry, such as the quenching of gas-phase radical channels, are not considered here. On the basis of similar specific surface area (Table 1), we conclude that the catalytic performance decreases in the order of $La_{1.85}Sr_{0.15}CuO_{3.930}Cl_{0.053} > La_{1.85}Sr_{0.15}CuO_{3.931}F_{0.060} > Nd_{1.85}Ce_{0.15}CuO_{3.981}F_{0.092} > Nd_{1.85}Ce_{0.15}CuO_{3.983}Cl_{0.068} \gg La_{1.85}Sr_{0.15}CuO_{3.934} \approx Nd_{1.85}Ce_{0.15}CuO_{3.980}$. The deep oxidation of C_2H_6 gives off much more heat than the ODE reaction. The variation trends of C_2H_6 conversion and C_2H_4 selectivity as related to contact time (Fig. 2) observed over $La_{1.85}Sr_{0.15}CuO_{3.930}Cl_{0.053}$ and $Nd_{1.85}Ce_{0.15}CuO_{3.981}F_{0.092}$ were similar to those obtained when the catalysts were well dispersed in quartz sand; the results demonstrate that the problem of hot spots in the catalyst bed was insignificant. In other words, the good performance observed is a result of catalytic actions of the halogen-containing Sr- or Ce-doped cuprate materials.

It should be noted that at reaction temperatures above 600°C, the halogenated catalysts showed a CH_4 selectivity in a range of 2–9%, whereas over the halogen-free catalysts no CH_4 was produced throughout the entire temperature range. The absence of CH_4 in the product mixtures indicates the strong total-oxidation ability of the $Ln_{1.85}A_{0.15}CuO_{4-\delta}$ catalysts. It might be associated with the existence of a higher oxygen vacancy density in the lattices. The formation of CH_4 requires the breaking of the C–C bond. As suggested by Kennedy and Cant (51), CH_4 generation follows two possible routes, i.e., C_2H_6 decomposition in the gas phase and a heterogeneous pathway involving an ethylperoxy intermediate. Ethylperoxy reacted with surface oxygen species to form CH_4 and HCO_2; the latter was further oxidized to CO_x.

It is well known that for perovskite-related oxide $A_2BO_{4-\delta}$, the rise in oxygen vacancy concentration (δ)

facilitates the total oxidation of hydrocarbons and that the enhancement in *B*-site ion redox ability is beneficial for the selective oxidation of hydrocarbons (10). Proper adjustment of the amounts of oxygen vacancies and the relative concentration of *B*-site ions would generate a perovskite-related material regulated for optimal catalytic performance. From the activity data in Figs. 1a–1f and the δ and σ values as well as the Cu^{3+} or Cu^{+} contents in Table 1, one may detect a specific bulk density of oxygen vacancy and a particular Cu^{3+} or Cu^{+} content in the best-performing halide-doped $Ln_{1.85}A_{0.15}CuO_{4-\delta}X_{\sigma}$ materials. The hole-doped halogen-containing cuprates performed superior to the electron-doped ones. This might be related to two factors: (i) the redox ability of Cu^{3+}/Cu^{2+} in the former is stronger than that of Cu^{2+}/Cu^{+} in the latter and (ii) the amount of oxygen vacancies in the former is more than that in the latter.

Due to the limited amounts of halogen intercalated, no obvious variations in crystal structure were detected. In other words, the $Ln_{1.85}A_{0.15}CuO_{4-\delta}X_{\sigma}$ catalysts retained a *T* or *T′* structure. The existence of a single-phase tetragonal $La_{1.85}Sr_{0.15}CuO_{3.930}Cl_{0.053}$ or $Nd_{1.85}Ce_{0.15}CuO_{3.981}F_{0.092}$ means that the two substances are thermally stable at the adopted reaction temperatures (i.e., below 700°C). The halogen contents of the fresh and used (after 60 h on-stream reaction) catalysts were rather similar (Table 1). The lifetime studies revealed that the halo-oxide catalysts were stable within a period of 60 h. These results suggested that both $La_{1.85}Sr_{0.15}CuO_{3.930}Cl_{0.053}$ and $Nd_{1.85}Ce_{0.15}CuO_{3.981}F_{0.092}$ are good and durable catalysts for the ODE reaction.

Defective Structure and Halogen Location

The pioneering work of Ovshinsky *et al.* (52) has given impetus to the investigation of the consequences of anion isomorphism in HTSCs. It is important to confirm the presence and location of halogen atoms in the crystal lattice. Works on fluorinated $YBa_2Cu_3O_{7-\delta}$ (53–56) manifest that the incorporated halogen atoms occupy the vacant oxygen positions in the Cu(1) plane where the Cu^{3+} ion is also located (57). Figure 8 shows the schematic structures of hole-doped $La_{2-x}Sr_xCuO_{4-\delta}$ (*T* structure) and electron-doped $Nd_{2-x}Ce_xCuO_{4-\delta}$ (*T′* structure) as well as their halide-incorporated counterparts. The crystal structure of cuprate HTSCs is characterized by the presence of Cu–O layers. The two-dimensional sheet structure of CuO_4 squares is indispensable to superconductivity, irrespective of the types of doped carriers, holes or electrons. An important structural difference between the hole-doped and the electron-doped HTSCs is the coordination of the Cu atoms. In the $La_{2-x}Sr_xCuO_{4-\delta}$ structure (Fig. 8I), the Cu atom is located in the center of a CuO_6 octahedron and the La and Sr atoms have ninefold coordinations, whereas in the $Nd_{2-x}Ce_x\ CuO_{4-\delta}$ structure (Fig. 8III) the Cu is in a square CuO_4 and the Nd and Ce atoms have nearly cubic eightfold

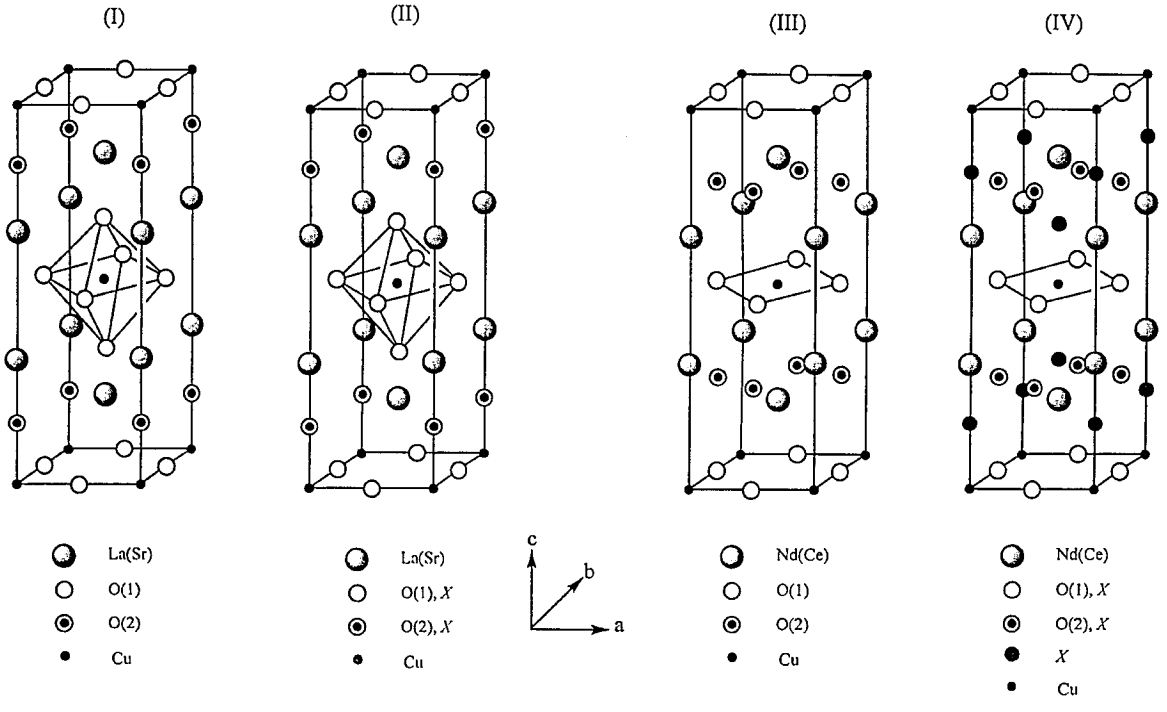

FIG. 8. Schematic structures of (I) $La_{2-x}Sr_xCuO_4$ (*T* structure), (II) $La_{2-x}Sr_xCuO_{4-\delta}X_{\sigma}$ (X = F, Cl) (*T* structure), (III) $Nd_{2-x}Ce_xCuO_4$ (*T′* structure), and (IV) $Nd_{2-x}Ce_xCuO_{4-\delta}X_{\sigma}$ (*T′* structure).

coordinations. As indicated in Fig. 8, there are two kinds of oxygen atoms [O(1)—apical oxygens—and O(2)]. Oxygen vacancies could be present at both O(1) and O(2) sites (58). The fractional occupancy at the O(2) site is slightly lower than that at the O(1) site (59). After investigating oxygen isotope $^{18}O/^{16}O$ exchange in $Nd_{1.85}Ce_{0.15}CuO_{4-\delta}$, Batlogg *et al.* (60) concluded that the isotope effect is small for all classes of cuprate HTSCs. Working on the $La_{1.85}Sr_{0.15}CuO_{4-\delta}$ material, Batlogg *et al.* (61) and Crawford *et al.* (62) demonstrated that ^{18}O substitution for ^{16}O occurs at both O(1) and O(2) sites. The observations of Al-Mamouri *et al.* (63) and the work by Weenk *et al.* based on Madelung energy calculation (64) reveal that F^- ions preferably occupy the apical sites [O(1)]. In addition, F^- ions can also enter into the interstitial sites (0, 1/2, 1/4) as reported in the case of $Sr_2CuO_2F_{2+\delta}$ (63). The occupation of O(1) sites by the doped halide ions has been confirmed by Chen *et al.*, who investigated a $La_{0.7}Sr_{1.3}Cu(O, F)_{4+\delta}$ HTSC material (35). By determining the lattice parameters of $Nd_2CuO_{4-x}F_x$, James *et al.* (32) pointed out that the doped F^- ions were located at the O(2) sites around the Nd^{3+} ions. However, Sugiyama *et al.* (34) and Krol *et al.* (65) considered that the doped F^- ions could occupy both the O(1) and O(2) sites. For the $La_{1.85}Sr_{0.15}CuO_{3.930}Cl_{0.053}$ and $Nd_{1.85}Ce_{0.15}CuO_{3.981}F_{0.092}$ catalysts, the halide ions could (i) replace some of the O^{2-} ions, (ii) occupy oxygen vacancies, or (iii) dwell at interstitial sites. If a F^- or Cl^- ion replaces an O^{2-} ion, in order to maintain electroneutrality, the oxidation state of an adjacent copper ion must drop from Cu^{3+} to Cu^{2+} or from Cu^{2+} to Cu^+; if a halide ion occupies an oxygen vacancy or an interstitial position, it would cause the oxidation state of an adjacent copper ion to rise from Cu^{2+} to Cu^{3+} or from Cu^+ to Cu^{2+}. From Table 1, one may observe that the doping of F^- or Cl^- ions caused the Cu^{3+} contents in $La_{1.85}Sr_{0.15}CuO_{4-\delta}$ and the Cu^{2+} contents (i.e., the decrease in Cu^+ content) in $Nd_{1.85}Ce_{0.15}CuO_{4-\delta}$ to increase rather than to decrease, demonstrating that the halide ions have occupied a certain amount of oxygen vacancies and/or interstitial spacings (66, 67). In the case of $La_{1.85}Sr_{0.15}CuO_{4-\delta}X_\sigma$ (Fig. 8II), the generation of Cu^{3+} ions would be induced by the preferential occupation of the originally vacant O(1) sites by X^- ions. In other words, the incorporated X^- ions dwelt at the O(1) sites in the CuO_6 octahedral plane of the *T* structure, forcing the oxidation state of the nearby copper ions to rise from Cu^{2+} to Cu^{3+}. In the case of $Nd_{1.85}Ce_{0.15}CuO_{4-\delta}X_\sigma$ (Fig. 8IV), however, the amount of halogen intercalated was larger than the available amount of oxygen vacancies; the introduced X^- ions were located mainly at the positions originally occupied by the O(2) and apical oxygens O(1) in the *T* structure (Fig. 8I) (which are vacant due to transformation from *T* to *T′* structure) as well as the interstitial spacings, driving the oxidation state of the nearby copper ions to rise from Cu^+ to Cu^{2+}.

Copper Oxidation States

La and Sr usually exist in +3 and +2 states in their compounds, respectively, but the oxidation state of Ce in CeO_2 or $Nd_{2-x}Ce_xCuO_{4-\delta}$ is controversial. Although there are claims that Ce is in a mixed-valence state in CeO_2 and in Ce-doped cuprates (68, 69), Wuilloud *et al.* (70) suggested that a "mixed valence" can be excluded in CeO_2 because of the observation of an empty localized Ce 4*f* state within the band gap in the bremsstrahlung isochromat spectroscopy data and no density of states was observed at the Fermi level in the XPS data. Based on the XPS results of cerium core levels, Hor *et al.* (71) believed that all of the cerium in $Nd_{2-x}Ce_xCuO_{4-\delta}$ is present as Ce^{4+}. Based on results of lattice parameters, Huang *et al.* (72) and Goodenough (73) pointed out that the valence of Ce in $Nd_{2-x}Ce_xCuO_{4-\delta}$ is not trivalent but tetravalent. In the present studies, a comparison between the Nd $3d_{5/2}$ spectra of Nd_2O_3 and the compounds Nd_2CuO_4, $Nd_{1.85}Ce_{0.15}CuO_{3.980}$ and $Nd_{1.85}Ce_{0.15}CuO_{3.981}F_{0.092}$ (Fig. 3I) and a comparison between the Ce 3*d* spectra of CeO_2 (Ce_2O_3 as well) and the compounds $Nd_{1.85}Ce_{0.15}CuO_{3.980}$ and $Nd_{1.85}Ce_{0.15}CuO_{3.981}F_{0.092}$ (Fig. 3II) clearly indicate that the Nd and Ce in the Ce-doped catalysts were in trivalency and tetravalency, respectively.

Although Kosugi *et al.* (74) stated that hole doping in $La_{2-x}Sr_xCuO_{4-\delta}$ occurs mainly at the oxygen site whereas electron doping takes place mainly at the Cu site of the CuO_4 plane in $Nd_{2-x}Ce_xCuO_{4-\delta}$, both kinds of doping would eventually bring about the changes in Cu oxidation state and oxygen vacancy density. For the hole-doped $La_{2-x}Sr_xCuO_{4-\delta}$ materials, there has not been a unified viewpoint on the oxidation state of Cu. Takahashi *et al.* (75), Rogers and Blair (76), and Ishii *et al.* (44) considered that Cu is divalent in $La_{2-x}Sr_xCuO_{4-\delta}$, Sarma and Rao (77) claimed to detect the presence of Cu^+; Rajadurai *et al.* (39), Subramanian and Swamy (38), Aleksandrov *et al.* (78), and Wu *et al.* (79) revealed that there were Cu^{3+} ions in $La_{2-x}Sr_xCuO_{4-\delta}$. As for $Nd_{2-x}Ce_xCuO_{4-\delta}$, the effect of Ce-doping on the valence of Cu is also debatable. Based on results of XPS studies, Uji *et al.* (80), Grassmann *et al.* (81), Liang *et al.* (82), and Suzuki *et al.* (83) reported that the Cu 2*p* spectra show the evidence of Cu^+ existence due to Ce substitution, but Rajumon *et al.* (84) considered it to be due to covalency effects. Based on X-ray absorption (XAS) data, Tranquada *et al.* (85) believed that the doped electrons fill the Cu 3*d* holes, but Alp *et al.* (86) argued that the electrons are injected into a band rather than distributed to Cu sites for Cu^+ formation.

By comparing the binding energies of the Cu $2p_{3/2}$ levels of Cu_2O, CuO, and La_4LiCuO_8 (Figs. 4a, 4b, and 4e), one can realize that there was only Cu^{2+} in Nd_2CuO_4 (Fig. 4c), indicating the absence of oxygen defects in the parent compound. The failure in detecting the signal of Cu^{3+} in

La_2CuO_4 (Fig. 4d) might be due to too low a concentration of Cu^{3+} in this sample. As shown in the Cu $2p_{3/2}$ spectra of $La_{1.85}Sr_{0.15}CuO_{3.934}$ and $La_{1.85}Sr_{0.15}CuO_{3.930}Cl_{0.053}$, the signal intensities of the shake-up satellite features as revealed by the I_s/I_m ratio in Table 3 increased with the rise in treatment temperature (Figs. 5IIIa–IIIc). It can be associated with the increase in Cu^{2+} concentration due to the desorption of oxygen species at elevated temperatures. For the Ce-doped catalysts, however, the trend was just the opposite (Figs. 5IVa–IVc and Table 3). It is due to the drop in Cu^{2+} content (i.e., the rise in Cu^{+} content). It has been suggested that the shake-up satellites observed in the Cu $2p_{3/2}$ spectra are caused by charge transfer from neighboring oxygen ligands into an empty *d* state of Cu^{2+} ion (87). Since the binding energy of the 2*p* electrons of Cu^{3+} ion should be larger than that of Cu^{2+} or Cu^{+} ion (44, 88), a peak at higher binding energy is expected for Cu^{3+}. From Figs. 5I and 5III, one can observe a shoulder peak around 934.6 eV, an indication of the presence of Cu^{3+} in the Sr-doped catalysts. The 934.6 eV signal decreased in intensity with the rise in temperature and disappeared at 700°C, indicating the decrease in concentration of Cu^{3+} ions upon heating of the catalysts in He. One can also see that in Fig. 5IV, the signal at ca. 932.7 eV due to Cu^{+} ion increased in intensity [in the meanwhile the I_s/I_m ratio decreased (Table 3)] with the increase in treatment temperature, signifying an increase in Cu^{+} content. The results of the analyses of copper oxidation state support the Cu^{3+} assignment. A similar Cu $2p_{3/2}$ feature has been reported by Ospett *et al.* (89) and Soderholm *et al.* (90), who confirmed the existence of trivalent copper ions in a $La_{1.85}Sr_{0.15}CuO_{4-\delta}$ sample based on the results of chemical analysis and XAS studies. The evidences for the presence of Cu^{+} ions in $Nd_{1.85}Ce_{0.15}CuO_{4-\delta}$ have also been reported before (80–83). The negative results in Cu^{+} analysis and the absence of signals due to Cu^{+} in our XPS analysis indicate the absence of Cu^{+} in the Sr-doped samples. This scenario is also true for the exclusion of Cu^{3+} in the Ce-doped samples. The above results confirm that there are only Cu^{2+} and Cu^{3+} ions in $La_{1.85}Sr_{0.15}CuO_{4-\delta}$ and $La_{1.85}Sr_{0.15}CuO_{4-\delta}X_\sigma$ and only Cu^{+} and Cu^{2+} ions in $Nd_{1.85}Ce_{0.15}CuO_{4-\delta}$ and $Nd_{1.85}Ce_{0.15}CuO_{4-\delta}X_\sigma$. It is well known that the ligand atoms in a compound could exert influence on the binding energy of the metal ions. The Cu $2p_{3/2}$ binding energies of $Ln_{1.85}A_{0.15}CuO_{4-\delta}X_\sigma$ are 0.6–0.7 eV lower than those of $Ln_{1.85}A_{0.15}CuO_{4-\delta}$. This difference might be due to the different ligand atoms of copper in the two series of catalysts.

Oxygen Activities

From the O 1*s* spectra (Fig. 6), one can observe that the O 1*s* binding energy of the lattice oxygen in $La_{1.85}Sr_{0.15}CuO_{3.930}Cl_{0.053}$ (529.8 eV) and $Nd_{1.85}Ce_{0.15}CuO_{3.981}F_{0.092}$ (529.6 ev) was 0.7–1.1 eV higher than that (528.7 eV) in $La_{1.85}Sr_{0.15}CuO_{3.934}$ and that (528.9 eV) in $Nd_{1.85}Ce_{0.15}CuO_{3.980}$, respectively. Due to the electronegativity of F (3.98) and Cl (3.16) (91), the intercalation of F or Cl into the $Ln_{1.85}A_{0.15}CuO_{4-\delta}$ lattice would cause the valence electron density of O^{2-} to decrease and the O 1*s* binding energy of O^{2-} to rise. It means that the presence of F or Cl in the *T* or *T′* lattice matrix would weaken the copper–oxygen bonds. Taking into account the fact that the O^{2-} [radius, 1.40 Å (92)] and F^{-} [radius, 1.38 Å (92)] ions are similar in size whereas the Cl^{-} [radius, 1.81 Å (92)] ions are somewhat larger than the O^{2-} ions, the F^{-} ions could enter into the $Ln_{1.85}A_{0.15}CuO_{4-\delta}$ lattice more readily than the Cl^{-} ions. As shown in Table 1, for the Ce-doped catalysts, the infiltration of F^{-} ions resulted in the shrinking of the *c*-axis and the elongation of the *a*- and *b*-axes, whereas the doping of Cl^{-} ions into $La_{1.85}Sr_{0.15}CuO_{4-\delta}$ induced the expansion of the *a*, *b*, and *c* dimensions (Table 1). Both effects would result in an increase in the Cu–O bond length (36). That means that the introduction of the halide ions would weaken the coulombic force between a copper ion and an O^{2-} ion. As a result, lattice O^{2-} would become more active. In other words, the inclusion of F^{-} or Cl^{-} ions in $Ln_{1.85}A_{0.15}CuO_{4-\delta}$ enhances the activity of lattice oxygen. The increase in C_2H_4 selectivity over the halide-doped $Ln_{1.85}A_{0.15}CuO_{4-\delta}X_\sigma$ catalysts (Figs. 1b and 1c) is supporting evidence for this viewpoint.

By determining the exact oxygen composition of $La_{1-x}Sr_xCoO_{3-\delta}$ ($x = 0$–1) before and after the respective desorption peaks, Yamazoe *et al.* concluded that a certain amount of Co^{4+} ion was actually induced by the oxygen dissociatively adsorbed at oxygen vacancies (93). Generally speaking, only after calcination in an O_2-containing atmosphere would the oxygen vacancies in a catalyst be occupied by dissociatively adsorbed oxygen (O^{-}). In the calcined $La_{1.85}Sr_{0.15}CuO_{4-\delta}$ catalyst, some Cu^{3+} ions were formed due to the occupancy of oxygen vacancies by O^{-}. Rao (94) pointed out that there were O^{-} species settling in the oxygen holes in $YBa_2Cu_3O_{7-\delta}$. The detection of the O 1*s* signal at ca. 531 eV (Fig. 6) indicates the presence of O^{-} in the Sr-doped cuprate catalysts. These results demonstrate that there were O^{-} species accommodated in the oxygen vacancies of the Sr-doped catalysts, driving the Cu^{3+} content to rise.

Both α- and β-oxygen desorptions in O_2-TPD profile are characteristics of most perovskites. The α-oxygen is accommodated in oxygen vacancies (93–96) and is responsible for the complete oxidation of hydrocarbons; the desorption of β-oxygen (i.e., lattice oxygen) is attributed to the partial reduction of *B*-site cation by lattice oxygen and is responsible for the selective oxidation of hydrocarbons (95, 96). The doping of F^{-} or Cl^{-} ions into the $Ln_{1.85}A_{0.15}CuO_{4-\delta}$ lattice would result in the decrease of α-oxygen (due to the decrease in the amount of oxygen vacancy) and the increase of β-oxygen desorption in the Sr-doped cuprates (due to

the rise in Cu^{3+} content) or the decrease of β-oxygen desorption in the Ce-doped cuprates (due to the drop in Cu^{+} content). As shown in Table 1, the addition of F^- or Cl^- ions into $La_{1.85}Sr_{0.15}CuO_{4-\delta}$ led to the increase rather than the decrease in Cu^{3+} content in the Sr-doped catalysts, indicating that the F^- or Cl^- ions have occupied a certain amount of oxygen vacancies in $La_{1.85}Sr_{0.15}CuO_{4-\delta}$, the doping of F^- or Cl^- ions to $Nd_{1.85}Ce_{0.15}CuO_{4-\delta}$ caused the Cu^{+} contents to decrease rather than to increase, indicating that the halide ions have occupied a certain amount of oxygen vacancies and interstitial spacings in $Nd_{1.85}Ce_{0.15}CuO_{4-\delta}$. The results of O_2-TPD studies clearly indicate that with the incorporation of F^- or Cl^- ions to $Ln_{1.85}A_{0.15}CuO_{4-\delta}$, the content of α-oxygen decreased (for $Nd_{1.85}Ce_{0.15}CuO_{3.981}F_{0.092}$, the desorption peak due to α-oxygen disappeared completely), whereas the content of β-oxygen increased for the Sr-doped catalyst and decreased for the Ce-doped catalyst; furthermore, the desorption temperature of the β-oxygen was obviously lowered. Therefore, we suggest that the decoration of $Ln_{1.85}A_{0.15}CuO_{4-\delta}$ with F^- or Cl^- ions has caused the bulk oxygen vacancy density to decline, thus reducing the complete oxidation reactions.

Obviously, the lattice oxygen in $La_{1.85}Sr_{0.15}CuO_{3.934}$ and $Nd_{1.85}Ce_{0.15}CuO_{3.980}$ was much less active than that in $La_{1.85}Sr_{0.15}CuO_{3.930}Cl_{0.053}$ and $Nd_{1.85}Ce_{0.15}CuO_{3.981}F_{0.092}$, respectively. These results indicate that the insertion of F^- or Cl^- ions into $Ln_{1.85}A_{0.15}CuO_{4-\delta}$ enhances the activity of lattice oxygen. When a C_2H_6 pulse was introduced, respectively, to $La_{1.85}Sr_{0.15}CuO_{3.934}$ and $Nd_{1.85}Ce_{0.15}CuO_{3.980}$ at 490 and 480°C, both catalysts showed C_2H_4 selectivities significantly lower than those observed over $La_{1.85}Sr_{0.15}CuO_{3.930}Cl_{0.053}$ and $Nd_{1.85}Ce_{0.15}CuO_{3.981}F_{0.092}$ (Table 5), confirming that the α-oxygen tends to induce the complete oxidation of C_2H_6. At 600 or 700°C, C_2H_6 conversion and C_2H_4 selectivity recorded either in a pulse of C_2H_6 or in a pulse of C_2H_6/O_2 increased noticeably over the four catalysts (Table 5), indicating that the β-oxygen (i.e., lattice oxygen) is accountable for the selective oxidation of C_2H_6 to C_2H_4. The evidence for direct involvement of lattice oxygen is from the isotope $^{18}O_2$-pulsing experiments performed over the $La_{1.85}Sr_{0.15}CuO_{3.930}Cl_{0.053}$ and $Nd_{1.85}Ce_{0.15}CuO_{3.981}F_{0.092}$ catalysts. Similar results were also observed over $YBa_2Cu_3O_{7-\delta}$ X_σ (X = F, Cl) (14). Considering that (i) O^- is much more reactive toward light hydrocarbons than O^{2-} (12, 14, 95, 96, 98, 99), (ii) the C_2H_6 conversions and C_2H_4 selectivities over the halogen-containing catalysts are higher than those over the halogen-free ones (Figs. 1a–1f and Table 5), and (iii) compared to the halide-doped cuprates, the undoped cuprates contained more O^- and less active lattice oxygen species (Figs. 6 and 7 and Table 4), one may conclude that in excessive amount, the O^- species at oxygen vacancies are prone to induce C_2H_6 deep oxidation, whereas the lattice O^{2-} species are responsible for C_2H_6 selective oxidation.

Copper Ion Redox Ability

As halide leaching was insignificant (Table 1), we consider that the weight losses observed in TGA studies were due to the desorption of oxygen species. From Table 3, one may assign the weight loss below 600°C to α-oxygen desorption (10):
for Sr-doped cuprates

$$Cu^{3+} + O^-_{vacancy} \rightarrow Cu^{2+} + (1/2)O_2, \quad [1]$$

for Ce-doped cuprates

$$Cu^{2+} + O^-_{vacancy} \rightarrow Cu^{+} + (1/2)O_2; \quad [2]$$

and those between 600 and 800°C to β-oxygen desorption (97):
for Sr-doped cuprates

$$2Cu^{3+} + O^{2-}_{lattice} \rightarrow 2Cu^{2+} + (1/2)O_2, \quad [3]$$

for Ce-doped cuprates

$$2Cu^{2+} + O^{2-}_{lattice} \rightarrow 2Cu^{+} + (1/2)O_2. \quad [4]$$

Generally speaking, the conversion of Cu^{3+} to Cu^{2+} is easier than that of Cu^{2+} to Cu^{+} because Cu^{2+} is more stable than Cu^{3+} or Cu^{+}. The latter process is difficult to take place in the Sr-doped catalysts. However, Ce^{4+} substitution for Nd^{3+} is beneficial for the stabilization of Cu^{+} in $Nd_{1.85}Ce_{0.15}CuO_{4-\delta}$. The doping of halide ions has been reported to be equally effective in stablizing Cu^{+} in $Nd_{1.85}Ce_{0.15}CuO_{4-\delta}$ (36). The decline in $O^-_{vacancy}$ dwelling in oxygen vacancies or the desorption of surface $O^{2-}_{lattice}$ would definitely lead to the increase of Cu^{+} content in the Ce-doped catalysts via Eq. [2] or [1]. From the results of O 1*s* and Cu 2$p_{3/2}$ studies, one can find that after H_2 treatment at 600°C, the O^- signals disappeared (Figs. 6III and 6IV) and Cu^{2+} concentration in $La_{1.85}Sr_{0.15}CuO_{3.930}Cl_{0.053}$ increased (Fig. 5III) whereas Cu^{2+} content in $Nd_{1.85}Ce_{0.15}CuO_{3.981}F_{0.092}$ decreased (Fig. 5IV), indicating that the removal of O^- species induced the occurrence of reaction [1] for the Sr-doped catalyst and reaction [2] for the Ce-doped catalyst. The approximation of weight losses below 600°C (Table 4) between the experimental and the theoretical values demonstrates that the α-oxygen in oxygen vacancies desorbed mostly via Eq. [2] or [1]. In the temperature range of 600–800°C, the weight losses of the two halogen-free catalysts were much less than those predicted theoretically, indicating that the reduction of Cu^{2+} to Cu^{+} was difficult. For $La_{1.85}Sr_{0.15}CuO_{3.930}Cl_{0.053}$, the weight loss observed was rather close to the theoretical value calculated according to Eq. [3], implying that the β-oxygen desorption was accompanied with Cu^{3+} reduction and the reduction of Cu^{2+} to Cu^{+} did not take place; however, for the $Nd_{1.85}Ce_{0.15}CuO_{3.981}F_{0.092}$

sample, the weight loss was only up to 8.1% of the theoretical value, indicating that a pronounced amount of Cu^{2+} was reduced to Cu^{+}, i.e., reaction [4] could occur in the Ce and F doubly doped catalyst. The changes in Cu^{3+} and Cu^{+} signals in the Cu $2p_{3/2}$ spectra of these catalysts with treatment temperatures also confirmed the above explanation.

Reaction Mechanism

Based on the changes in Cu^{3+} or Cu^{+} content in thermal treatment, ^{18}O- and C_2H_6-pulsing studies and according to the nature of oxygen species discussed in the TGA and O_2-TPD sections as well as the results reported by Subramanian and Swamy (38), Kennedy and Cant (51), and Lunsford and co-workers (98, 99), we propose the following reaction steps for the Sr-doped cuprate catalysts:

$$Cu^{3+}\text{–}O^{-}\text{–}Cu^{2+} + C_2H_6 \rightarrow Cu^{2+}\text{–}\square\text{–}Cu^{2+} + C_2H_5^{\bullet} + OH^{-} \quad [5]$$

$$Cu^{3+}\text{–}O^{2-}\text{–}Cu^{2+} + C_2H_5^{\bullet} \rightarrow Cu^{2+}\text{–}\square\text{–}Cu^{2+} + C_2H_5O^{-} \quad [6]$$

$$Cu^{2+}\text{–}\square\text{–}Cu^{2+} + (1/2)O_2 \rightarrow Cu^{3+}\text{–}O^{-}\text{–}Cu^{2+} \quad [7]$$

$$Cu^{3+}\text{–}O^{-}\text{–}Cu^{2+} \rightarrow Cu^{3+}\text{–}O^{2-}\text{–}Cu^{2+} + e \quad [8]$$

$$C_2H_5O^{-} \rightarrow C_2H_4 + OH^{-} \quad [9]$$

$$C_2H_5O^{-} + OH^{-} \rightarrow C_2H_4 + H_2O + O^{2-} \quad [10]$$

$$Cu^{3+}\text{–}O^{2-}\text{–}Cu^{2+} + C_2H_6 + e \rightarrow Cu^{2+}\text{–}\square\text{–}Cu^{2+} + C_2H_4 + H_2O \quad [11]$$

$$Cu^{2+}\text{–}\square\text{–}Cu^{2+} + O^{2-} \rightarrow Cu^{3+}\text{–}O^{2-}\text{–}Cu^{2+} + e \quad [12]$$

$$Cu^{3+}\text{–}O^{-}\text{–}Cu^{2+} + C_2H_5O^{-} \rightarrow Cu^{2+}\text{–}\square\text{–}Cu^{2+} + CO_x + CH_4 + H_2O. \quad [13]$$

The O^{-} species located at oxygen vacancies abstract a hydrogen atom from C_2H_6 to form $C_2H_5^{\bullet}$ species (Step [5]) which react with $O^{2-}_{lattice}$ species to give surface ethoxide ($C_2H_5O^{-}$) (Step [6]) or lose another hydrogen atom to generate a small amount of C_2H_4 (Step [9]) at lower temperatures (98, 99). Subsequent interaction of ethoxide with OH^{-} at higher temperatures produces a larger amount of C_2H_4 (Step [10]). The direct reaction of $O^{2-}_{lattice}$ with C_2H_6 to form C_2H_4 (Step [11]) and the further oxidation of ethoxide by an excessive amount of O^{-} species would lead to the breakage of C–C bond, generating CO_x and CH_4 as a result (Step [13]) (51, 98, 99). The redox cycle of Cu^{3+}/Cu^{2+} ions (Steps [5]–[8] and [11]–[13]) undergoes with the redox process of oxygen (Steps [5]–[8] and [10]–[12]). The consumed O^{-} or O^{2-} species in the catalysts are replenished by the oxygen from the gas phase (Steps [7] and [8]). Reaction pathways are expected to be similar over the Ce-doped cuprate catalysts, except that the symbols of Cu ions should be Cu^{2+}–O^{-}–Cu^{+}, Cu^{+}–□–Cu^{+}, and Cu^{2+}–O^{2-}–Cu^{+}, accordingly. From the above reaction steps, one can see that certain amounts of O^{-} and active lattice O^{2-} are required for the redox cycle. We speculate that the pathways of O_2 activation over these two kinds of catalysts are different: due to the very fact that only a limited amount of oxygen vacancies is available in the fluorinated Ce-doped cuprate catalyst, O_2 might be activated to form O^{-} via the oxidation of Cu^{+} to Cu^{2+}; whereas in the chlorinated Sr-doped cuprate catalyst, due to the relatively higher availability in oxygen vacancy, the activation of O_2 might follow the sequence: Steps [5] → [6] → [7] → [8].

CONCLUSIONS

The hole-doped $La_{1.85}Sr_{0.15}CuO_{4-\delta}$ and $La_{1.85}Sr_{0.15}CuO_{4-\delta}X_{\sigma}$ catalysts performed better than the electron-doped $Nd_{1.85}Ce_{0.15}CuO_{4-\delta}$ and $Nd_{1.85}Ce_{0.15}CuO_{4-\delta}X_{\sigma}$ (X = F, Cl) for the ODE reaction. $La_{1.85}Sr_{0.15}CuO_{3.930}Cl_{0.053}$ and $Nd_{1.85}Ce_{0.15}CuO_{3.981}F_{0.092}$ exhibited the best performance in each of the two series of catalysts. Both of them showed stable performance during a period of 60 h on-stream reaction at 660°C. XRD results indicated that the Sr-substituted cuprates were of T structure, whereas the Ce-doped cuprates were of T' structure. XPS studies illustrate that there were Cu^{2+} and Cu^{3+} in the former catalysts and Cu^{+} and Cu^{2+} in the latter catalysts. Hole doping induces the generation of Cu^{3+} in the Sr-substituted catalysts, whereas electron doping brings about the formation of Cu^{+} in the Ce-substituted catalysts. The inclusion of halide ions in the $Ln_{1.85}A_{0.15}CuO_{4-\delta}$ (Ln = La, Nd; A = Sr, Ce) lattice enhanced lattice oxygen activity. Based on the results of XPS, TGA, O_2-TPD, and ^{18}O- and C_2H_6-pulsing experiments as well as catalytic activities, we conclude that (i) surface lattice O^{2-} species are responsible for ethane selective oxidation; (ii) in excessive amount, the O^{-} species located at oxygen vacancies induce ethane deep oxidation; and (iii) a proper Cu^{3+}/Cu^{2+} couple concentration and oxygen vacancy density in $La_{1.85}Sr_{0.15}CuO_{4-\delta}X_{\sigma}$ or Cu^{2+}/Cu^{+} pair content and/or oxygen vacancy density in $Nd_{1.85}Ce_{0.15}CuO_{4-\delta}X_{\sigma}$ (X = F, Cl) are necessary for the best catalytic performance of the catalysts.

ACKNOWLEDGMENTS

The work described above was fully supported by a grant from the Research Grants Council of the Hong Kong Special Administration Region, People's Republic of China (Project No. HKBU 2015/99P). H. X. Dai thanks the HKBU for a Ph.D. studentship.

REFERENCES

1. Conway, S. J., Wang, D. J., and Lunsford, J. H., *Appl. Catal. A* **79**, L1 (1991).
2. McCain, J. H., U.S. Patent 4 524 236 (1985).
3. Wang, S. B., Murata, K., Hayakawa, T., Hamakawa, S., and Suzuki, K., *Catal. Lett.* **59**, 173 (1999).

4. Ueda, W., Lin, S. W., and Tohmoto, I., *Catal. Lett.* **44**, 241 (1996).
5. Omata, K., Yamazaki, O., Tomita, K., and Fujimoto, K., *J. Chem. Soc. Chem. Commun.*, 1647 (1994).
6. Lin, Y. S., and Zeng, Y., *J. Catal.* **164**, 220 (1996).
7. ten Helshof, J. E., Bouwmeester, H. J. M., and Verweeij, H., *Appl. Catal. A* **130**, 195 (1995).
8. Alcock, C. B., Carberry, J. J., Doshi, R., and Gunasekaran, N., *J. Catal.* **143**, 533 (1993).
9. Yi, G. H., Hayakawa, T., Anderson, A. G., Suzuki, K., Hamakawa, S., York, A. P. E., Shimizu, M., and Takehira, K., *Catal. Lett.* **38**, 189 (1996).
10. Seiyama, T., *in* "Properties and Application of Perovskite-Type Oxides" (L. G. Tejuca and J. L. G. Fierro, Eds.). Dekker, New York, 1993.
11. Viswanathan, B., *in* "Properties and Application of Perovskite-Type Oxides" (L. G. Tejuca and J. L. G. Fierro, Eds.). Dekker, New York, 1993.
12. Dai, H. X., Ng, C. F., and Au, C. T., *J. Catal.* **189**, 52 (2000).
13. Dai, H. X., Ng, C. F., and Au, C. T., *Catal. Lett.* **57**, 115 (1999).
14. Dai, H. X., Ng, C. F., and Au, C. T., *J. Catal.* **193**, 65 (2000).
15. Bednorz, J. G., and Müller, K. A., *Z. Phys.* **64**, 189 (1986).
16. Tokura, Y., Takagi, H., and Uchida, S., *Nature* **337**, 345 (1989).
17. Cava, R. J., van Dover, R. B., Batlogg, B., and Rietman, E. A., *Phys. Rev. Lett.* **58**, 408 (1987).
18. Alp, E. E., Shenoy, G. K., Hinks, D. G., Capone, D. W., II, Soderholm, L., and Schuttler, H. B., *Phys. Rev. B: Condens. Matter* **35**, 7199 (1987).
19. Torrance, J. B., Bezings, A., Nazzai, A. I., Huang, T. C., Parkin, S. S. P., Keane, O. T., Laplaca, S. J., Horn, P. M., and Helo, G. A., *Phys. Rev. B* **40**, 8872 (1989).
20. Hidaka, Y., and Suzuki, M., *Nature* **338**, 635 (1989).
21. Takagi, H., Uchida, S., and Tokura, Y., *Phys. Rev. Lett.* **62**, 1197 (1989).
22. Fortune, N. A., Murata, K., Ishibashi, M., Yokoyama, Y., and Nishihara, Y., *Physica B* **169**, 635 (1991).
23. Klauda, M., Ströbel, J. P., Schlötterer, J., Grassmann, A., Markl, J., and Saemann-Ischenko, G., *Physica C* **173**, 109 (1991).
24. Fortune, N. A., Murata, K., Yokoyama, Y., Ishibashi, M., and Nishihara, Y., *Physica C* **178**, 437 (1991).
25. Uji, S., and Aoki, H., *Physica C* **199**, 231 (1992).
26. Prasad Beesabathina, D., Salamanca-Riba, L., Peng, J. L., Li, Z. Y., and Greene, R. L., *Physica C* **208**, 79 (1993).
27. Kawashima, T., and Takayama-Muromachi, E., *Physica C* **219**, 389 (1994).
28. Makarova, I. P., Bram, A., Markl, J., Gamaunov, K. V., Ivanov, A. L., Tamazyan, R. A., Röhner, M., Burzlaff, H., Saemann-Ischenko, G., Simonov, V. I., and Osiko, V. V., *Physica C* **223**, 1 (1994).
29. Zhu, Y. T., and Manthiram, A., *Physica C* **224**, 256 (1994).
30. Yamamoto, H., Naito, M., and Sato, H., *Physica C* **291**, 67 (1997).
31. Kim, J. S., and Kvam, E. P., *Physica C* **292**, 203 (1997).
32. James, A. C. W. P., Zahurak, S. M., and Murphy, D. W., *Nature* **338**, 240 (1989).
33. Sugiyama, J., Ojima, Y., Takata, T., Sakuyama, K., and Yamauchi, H., *Physica C* **173**, 103 (1991).
34. Sugiyama, J., Kosuge, M., Ojima, Y., Yamauchi, H., and Tanaka, S., *Physica C* **179**, 131 (1991).
35. Chen, X., Liang, J., Tang, W., Wang, C., and Rao, G., *Phys. Rev. B* **52**, 16233 (1995).
36. Asaf, U., Felner, I., and Yaron, U., *Physica C* **211**, 45 (1993).
37. Christopher, J., and Swamy, C. S., *J. Mol. Catal.* **62**, 69 (1990).
38. Subramanian, S., and Swamy, C. S., *Catal. Lett.* **35**, 361 (1995).
39. Rajadurai, S., Carberry, J. J., Li, B., and Alcock, C. B., *J. Catal.* **131**, 582 (1991).
40. Lee, I., and Ng, K. Y. S., *Catal. Lett.* **2**, 403 (1989).
41. Au, C. T., Liu, Y. W., and Ng, C. F., *J. Catal.* **176**, 365 (1998).
42. Fuggle, J. C., Campagna, M., Zolnierek, Z., Lasser, R., and Piatau, A., *Phys. Rev. Lett.* **45**, 1597 (1980).
43. Rao, C. N. R., and Sarma, D. D., *in* "Science and Technology of Rare Earths" (E. C. Subbarao and W. E. Wallance, Eds.). Academic Press, New York, 1980.
44. Ishii, H., Koshizawa, T., Kataura, H., Hanyu, T., Takai, H., Mizoguchi, K., Kume, K., Shiozaki, I., and Yamaguchi, S., *Jpn. J. Appl. Phys., Part 2* **28**, L1952 (1989).
45. Choy, J. H., Jung, D. Y., Kim, S. J., Choi, Q. W., and Demazeau, G., *Physica C* **185–189**, 763 (1991).
46. Kulkarni, G. U., Rao, C. N. R., and Roberts, M. W., *J. Phys. Chem.* **99**, 3310 (1995).
47. Carley, A. F., Roberts, M. W., and Santra, A. K., *J. Phys. Chem. B* **101**, 9978 (1997).
48. Yamazoe, N., Teraoka, Y., and Seiyama, T., *Chem. Lett.*, 1767 (1981).
49. Fierro, J. L. G., and Tejuca, L. G., *Appl. Surf. Sci.* **27**, 453 (1987).
50. Shi, C., Rosynek, M. P., and Lunsford, J. H., *J. Phys. Chem.* **98**, 8371 (1994).
51. Kennedy, E. M., and Cant, N. W., *Appl. Catal.* **75**, 321 (1991).
52. Ovshinsky, S. R., Young, R. T., Allred, D. D., Demaggio, G., and van der Leeden, G. A., *Phys. Rev. Lett.* **58**, 2579 (1987).
53. LaGraff, J. R., Behrman, E. C., Taylor, J. A. T., Rotella, E. J., Jorgensen, J. D., Wang, L. Q., and Mattocks, P. G., *Phys. Rev. B* **39**, 347 (1989).
54. Perrin, C., Dinia, A., Pena, O., Sergent, M., Burlet, P., and Rossat-Mignod, J., *Solid State Commun.* **76**, 401 (1990).
55. Nemudry, A. P., Pavlyukhin, Y. T., Khainovskii, N. G., and Boldyrev, V. V., *Superconductivity* **3**, 1528 (1990).
56. Ossipyan, Yu. A., Zharikov, O. V., Logvenov, G. Yu, Sidorov, N. S., Kulakov, V. I., Shmytko, I. M., Bdikin, I. K., and Gromov, A. M., *Physica C* **165**, 107 (1990).
57. David, W. I. F., Harrison, W. T. A., Gunn, J. M. F., Moze, O., Soper, A. K., Day, P., Jorgensen, J. D., Hinks, D. G., Beno, M. A., Soderholm, L., Capone, D. W., II, Schuller, I. K., Segre, C. U., Zhang, K., and Grace, J. D., *Nature* **327**, 310 (1987).
58. Izumi, F., Matsui, Y., Takagi, H., Tokura, Y., and Asano, H., *Physica C* **158**, 433 (1989).
59. Kwei, G. H., Cheong, S. W., Fisk, Z., Garzon, F. H., Goldstone, J. A., and Thompson, J. D., *Phys. Rev. B* **40**, 9370 (1989).
60. Batlogg, B., Cheong, S. W., Thomas, G. A., Cooper, S. L., Rupp, L. W., Jr., Rapkine, D. H., and Cooper, A. S., *Physica C* **185–189**, 1385 (1991).
61. Batlogg, B., Kourouklis, G., Weber, W., Cava, R. J., Jayaraman, A., White, A. E., Short, K. T., Rupp, L. W., and Rietman, E. A., *Phys. Rev. Lett.* **59**, 912 (1987).
62. Crawford, M. K., Kunchur, M. N., Farneth, W. E., McCarron, E. M., III, and Poon, S. J., *Phys. Rev. B: Condens. Matter* **41**, 282 (1990).
63. Al-Mamouri, M., Edwards, P. P., Greaves, C., and Slaski, M., *Nature* **369**, 382 (1994).
64. Weenk, J. W., and Harwig, H. A. T., *Phys. Chem. Solids* **38**, 1047 (1977).
65. Krol, A., Soo, Y. L., Ming, Z. H., Huang, S., Kao, Y. H., Smith, G. C., Lee, K., James, A. C. W. P., and Murphy, D. W., *Phys. Rev. B* **46**, 443 (1992).
66. Bhat, V., Rao, C. N. R., and Honig, J. M., *Solid State Commun.* **81**, 751 (1992).
67. Tatsuki, T., Adachi, S., Tamura, T., and Tanabe, K., *Physica C* **303**, 41 (1998).
68. Koelling, D. D., Boring, A. M., and Wood, J. H., *Solid State Commun.* **47**, 227 (1983).
69. Kotani, A., Mizuta, H., Jo, T., and Parlebas, J. C., *Solid State Commun.* **53**, 805 (1985).
70. Wuilloud, E., Delley, B., Schneider, W. D., and Bear, Y., *Phys. Rev. Lett.* **53**, 202 (1984).
71. Hor, P. H., Xue, Y. Y., Sun, Y. Y., Tao, Y. C., Huang, Z. J., Rabalais, W., and Chu, C. W., *Physica C* **159**, 629 (1989).
72. Huang, T. C., Moran, E., Nazzal, A. I., and Torrance, J. B., *Physica C* **158**, 148 (1989).
73. Goodenough, J. B., *Supercond. Sci. Technol.* **3**, 26 (1990).

74. Kosugi, N., Tokura, Y., Tagaki, H., and Uchida, S., *Phys. Rev. B* **41**, 131 (1990).
75. Takahashi, T., Maeda, F., Miyahara, T., Hosoya, S., and Sato, M., *Jpn. J. Appl. Phys., Part 1* **26**, 1013 (1987).
76. Rogers, J. W., Jr., and Blair, D. S., *AIP Conf. Proc.* **165**, 323 (1988).
77. Sarma, D. D., and Rao, C. N. R., *J. Phys. C: Solid State Phys.* **20**, L659 (1987).
78. Aleksandrov, A. S., Lebedinskii, Yu. Yu., Protasov, E. A., and Chubunova, E. V., *Pis'ma Zh. Eksp. Teor. Fiz.* **46**, 180 (1987).
79. Wu, Y., Gao, L. Z., and Yu, Z. L., *Huaxue Xuebao* **55**, 56 (1997).
80. Uji, S., Shimoda, M., and Aoki, H., *Jpn. J. Appl. Phys.* **28**, L804 (1989).
81. Grassmann, A., Schlötterer, J., Ströbel, J., Klanda, M., Johnson, R. L., and Saemann-Ischenko, G., *in* "Proc. Intern. Conf. Mater. Mechanism Supercond. High-Temp. Supercond. II" (N. E. Phillips, R. N. Shelton, and W. A. Harrison, Eds.). North-Holland, Amsterdam, 1989.
82. Liang, G., Chen, J., Croft, M., Ramanujachary, K. V., Greenblatt, M., and Hedge, M., *Phys. Rev. B* **40**, 2646 (1989).
83. Suzuki, T., Nagoshi, M., Fukuda, Y., Oh-ishi, K., Syono, Y., and Tachiki, M., *Phys. Rev. B* **42**, 4263 (1990).
84. Rajumon, M. K., Sarma, D. D., Vijayaraghavan, R., and Rao, C. N. R., *Solid State Commun.* **70**, 875 (1989).
85. Tranquada, J. M., Heald, S. M., Moodenbaugh, A. R., Liang, G., and Groft, M., *Nature* **337**, 720 (1989).
86. Alp, E. E., Mini, S. M., Ramanathan, M., Dabrowski, B., Richards, D. R., and Hinks, D. G., *Phys. Rev. B* **40**, 2617 (1989).
87. Kim, K. S., *J. Electron. Spectrosc.* **3**, 217 (1974).
88. Shin, J. S., Enomoto, H., Takauchi, H., Takno, Y., Mori, N., and Ozaki, H., *Jpn. J. Appl. Phys.* **28**, L1365 (1989).
89. Ospett, M., Henz, J., Kaldis, E., and Wachter, P., *Physica C* **153–155**, 159 (1988).
90. Soderholm, L., Alp, E. E., Beno, M. A., Morss, L. R., Shenoy, G., and Goodman, G. L., *in* "High Temperature Superconductivity Materials" (W. E. Hatfield and J. H. Miller, Jr., Eds.). Dekker, New York, 1988.
91. Cotton, F. A., and Wilkinson, G., "Advanced Inorganic Chemistry," 3rd ed. Interscience, New York, 1972.
92. Lide, D. R. (Ed.), "Handbook of Chemistry and Physics." CRC Press, New York, 1998–1999.
93. Yamazoe, N., Teraoka, Y., and Seiyama, T., *Chem. Lett.*, 1767 (1981).
94. Rao, C. N. R., *in* "Chemistry of Oxide Superconductivity" (C. N. R. Rao, Ed.). Blackwell, Oxford, 1988.
95. Bielañski, A., and Haber, J., "Oxygen in Catalysis." Dekker, New York, 1991.
96. Haber, J., *in* "Surface Properties and Catalysis by Non-Metals" (J. P. Bonnelle, B. Delmon, and E. Derouane, Eds.). Reidel, Dordrecht, 1983.
97. Wu, Y., Yu, T., Dou, B. S., Wang, C. X., Xie, X. F., Yu, Z. L., Fan, S. R., Fan, Z. R., and Wang, L. C., *J. Catal.* **120**, 88 (1989).
98. Aika, K. I., and Lunsford, J. H., *J. Phys. Chem.* **81**, 1393 (1977).
99. Aika, K. I., and Lunsford, J. H., *J. Phys. Chem.* **82**, 1794 (1978).